Response of phytoplankton functional types to Hurricane Fabian (2003) in the Sargasso Sea

Dailé Avila-Alonso[*1,2], Jan M. Baetens[2], Rolando Cardenas[1], Bernard De Baets[2]

[1]Planetary Science Laboratory, Department of Physics, Universidad Central "Marta Abreu" de Las Villas, 54830, Santa Clara, Villa Clara, Cuba.

[2]KERMIT, Department of Data Analysis and Mathematical Modelling, Faculty of Bioscience Engineering, Ghent University, 9000 Ghent, Belgium.

*Corresponding author email: daile.avilaalonso@gmail.com

Running Title: Phytoplankton community response to Hurricane Fabian

ABSTRACT

Understanding how tropical cyclones affect phytoplankton communities is important for studies on ecological variability. Most studies assessing the post-storm phytoplankton response rely on satellite observations of chlorophyll *a* concentration, which inform on the ocean surface conditions and the whole phytoplankton community. In this work, we assess the potential of the Massachusetts Institute of Technology marine ecosystem model to account for the response of individual phytoplankton functional types (PFTs, coccolithophores, diatoms, diazotrophs, mixotrophic dinoflagellates, picoeukaryotes, *Prochlorococcus* and *Synechococcus*) in the euphotic zone to the passage of Hurricane Fabian (2003) across the tropical and subtropical Sargasso Sea. Fabian induced a significant mean concentration increase (t-test, $p < 0.05$) of all PFTs in the tropical waters (except for *Prochlorococcus*), which was driven by the mean nutrient concentration increase and by a limited zooplankton grazing pressure. More specifically, the post-storm nutrient enrichment increased the contribution of fast-growing PFTs (e.g. diatoms and coccolithophores) to the total phytoplankton concentration and decreased the contribution of slow-growing dominant

groups (e.g. picoeukaryotes, *Prochlorococcus* and *Synechococcus*), which lead to a significant increase (t-test, $p < 0.05$) of the Shannon diversity index values. Overall, the model captured the causal relationship between nutrient and PFT concentration increases in the tropical waters, although it only reproduced the most pronounced PFT responses such as those in the deep euphotic zone. In contrast, the model did not capture the oceanic perturbations induced by Fabian as observed in satellite imagery in the subtropical waters, probably due to its limited performance in this complex oceanographic area.

Keywords: diversity, major hurricane, modelling, phytoplankton community, remote sensing

1. INTRODUCTION

The open ocean accounts for nearly 70% of Earth's surface and represents the largest habitat in the biosphere. Phytoplankton, which are responsible for about half of the total primary production at planetary scale (Field et al. 1998), directly or indirectly, support ocean life. The productivity and diversity of phytoplankton determine the structure and functioning of planktonic communities in general (Striebel et al. 2012, Otero et al. 2020). Besides, phytoplankton modulate fishing yields and global biogeochemical cycles (Chassot et al. 2010, Litchman et al. 2015, Marshak & Link 2021). Evidence for the impact of climate change on the marine environment is becoming increasingly clear in, for example, the North Atlantic, a key region for carbon sequestration (Gruber et al. 2002, Garcia-Soto et al. 2021). Therefore, understanding the phytoplankton response to environmental variability is crucial (Estrada et al. 2016), especially for understanding the functioning of marine ecosystems in short-term physical processes (Stanichny et al. 2021).

Tropical cyclones (TCs), such as hurricanes, typhoons, tropical storms or tropical depressions, are extreme storms that substantially perturb oceans (Price 1981, Babin et al. 2004, Naik et al. 2008). These sudden environmental disturbances impact marine ecosystems and lead to

patches of high primary and secondary production (Fiedler et al. 2013). TC forcing leads to strong vertical mixing and upwelling leading to entrainment of nutrient-rich deep waters into the upper ocean, which fuels phytoplankton production (Walker et al. 2005, Gierach & Subrahmanyam 2008). For instance, TC-induced mixing can extend at least 80 m below the base of the mixed layer in the subtropical North Atlantic (Zedler et al. 2002), while the induced inertial waves can propagate up to 2000 m depth (Morozov & Velarde 2008). Thus, the cyclone-induced mixing can reach the nitracline located between 90–150 m in summer in the northern Sargasso Sea (Malone et al. 1993, Goericke & Welschmeyer 1998), leading to a large supply of nutrients into the surface ocean layer (Foltz et al. 2015).

Motivated by the increased TC activity over the past decades (Deo et al. 2011), considerable efforts have been devoted to investigate the impact of TCs on marine phytoplankton (Anglès et al. 2015). This is particularly relevant in the North Atlantic Basin, one of the most active TC regions around the world, where the largest positive trend in TC intensity has been reported in the last decades (Kossin et al. 2020). Studies in this TC-prone region have used satellite observations of chlorophyll (Chl) *a* concentration mainly as a proxy for phytoplankton biomass in order to assess the phytoplankton post-storm variability (e.g. Babin et al. 2004, Foltz et al. 2015, Shropshire et al. 2016, Avila-Alonso et al. 2021). Satellite-based observations are suitable to assess the oceanographic variability at high spatial and temporal resolution and are valuable sources of information to further the understanding of the TC-induced oceanographic variability (Son et al. 2007). However, satellite ocean colour data only provide information on the ocean surface (first optical depth, which is 4.6 times shallower than the euphotic depth) (Gordon & McCluney 1975, Kirk 2011). Even though a post-storm surface Chl *a* concentration increase can typically be detected by satellite sensors, it may as well reflect a vertical redistribution of the subsurface Chl *a* maximum (physical transport of biomass)

instead of an increase of surface phytoplankton production as a consequence of nutrient enrichment (intrinsic biological response) (Painter et al. 2016).

On the other hand, satellite Chl *a* concentration largely accounts for the whole phytoplankton community since Chl *a* is an omnipresent pigment in all phytoplankton species (Jeffrey & Vesk 1997). However, the response of the phytoplankton community to nutrient increase ultimately depends on each taxon's unique nutrient requirements, which are influenced by their specific resource utilization strategies, growth rates, cell size, traits, etc. (e.g. Geider & La Roche 2002, Litchman et al. 2007, Marañon et al. 2013, Bonachela et al. 2016). Thus, a post-storm assessment of the phytoplankton response should consider, at least, the individual responses of the major phytoplankton functional types (PFTs, aggregates of organisms with common biogeochemical functions; Follows & Dutkiewicz 2011) in the upper ocean layer to get a deeper understanding of the biological perturbations induced by these phenomena. However, such studies have been limited because of data availability.

Overall, in situ, satellite and/or modelled data might be used to assess the post-storm response of functional and/or taxonomic associations of phytoplankton. Although in situ data provide accurate information on environmental changes, traditional sampling techniques are time consuming, weather dependent and provide information on a limited geographic area (Painter et al. 2016). Besides, many oceanic regions are so remote that they cannot be monitored routinely and, therefore, data on oceanic phytoplankton communities after TC passage are limited (Mangesh et al. 2016). More specifically, in situ observations on appropriate space/time scales are lacking to study the effect of storms on the phytoplankton communities in the western Sargasso Sea. On the other hand, although several methods to assess phytoplankton diversity from ocean colour satellite observations have been developed for over two decades, applications of these datasets have been limited (IOCCG 2014, Bracher

et al. 2017). This is mainly due to the mismatch between satellite, in situ and modelled data on phytoplankton composition, the spectral limitation of current multi-spectral sensors, and the very limited applicability of these algorithms at regional scale (IOCCG 2014). Additionally, as was mentioned above, ocean colour data only provide information on the surface ocean, hence most satellite-based PFT algorithms account for surface phytoplankton communities as well (IOCCG 2014, Bracher et al. 2017).

Alternatively, coupled biogeochemical-ocean general circulation models produce three-dimensional projections of PFTs, considering functions of light, nutrients, temperature, salinity, etc., influencing their growth and abundance (for more details, see Fig. 2 in Bracher et al. 2017). Despite the limitations of aquatic biogeochemical models to reproduce the dynamics of PFTs across a wide range of temporal and spatial scales (Shimoda & Arhonditsis, 2016), such models are suited to assess the regulation pattern of marine microbe biodiversity, and to simulate the response to changing environments (Follows & Dutkiewicz 2011). Data derived from these models (i.e. the model outputs) are often publicly available (e.g. Jahn et al. 2019), which allows to assess the potential of the underlying model to investigate specific oceanic responses. This type of preliminary/exploratory study can stimulate and guide future research to improve the model performance in specific oceanic areas.

In this paper, we assess the potential of the Massachusetts Institute of Technology (MIT) coupled physical-biogeochemical ecosystem model (from now on called MIT marine ecosystem model for ease of reference) to capture the post-storm response of PFTs in the euphotic zone to the passage of Hurricane Fabian (2003) across the western Sargasso Sea in the North Atlantic (Fig. 1A) using publicly available model outputs. Fabian was an exceptionally long-lived and intense hurricane (Lawrence et al. 2005) (Fig. 1B). The Fabian-induced physical and biological oceanographic variability has been widely studied (e.g. Son et

al. 2007, Black & Dickey 2008, Price et al. 2008, Pedrosa-Pàmies et al. 2019). This provides a consistent background to support and evaluate our results. To our knowledge, this is the first time that PFTs are incorporated in an analysis of the post-storm response of a phytoplankton community in the western Sargasso Sea. We first present a brief description of the Fabian and the methods used, including the datasets containing the relevant physical and biological variables (Section 2). In Section 3, we present a model validation together with the modelled phytoplankton community response to the passage of Fabian, followed by a discussion of the storm-induced variability and the model performance in general (Section 4).

2. MATERIALS & METHODS

2.1. Synoptic history of Fabian and study area

Fabian evolved from a tropical wave that originated from western Africa on 25 August 2003 and moved westward becoming a tropical depression on 27 August at 676 km west of the Cape Verde Islands (Pasch et al. 2003). With favourable atmospheric and oceanic conditions, this TC strengthened and became a tropical storm on 28 August and a hurricane two days later over the east-central tropical Atlantic (Pasch et al. 2003). Its highest intensity (64 m s^{-1}, category 4 (H4) on the Saffir Simpson Hurricane Scale) was reached on 1 September (Pasch et al. 2003, Lawrence et al. 2005). Fabian struck Bermuda island on 5 September with winds of 51 m s^{-1} and then accelerated northeastward while starting to weaken (Pasch et al. 2003, Lawrence et al. 2005) (Fig. 1B). Overall, Fabian followed a nearly meridional trajectory across the deep oceanic waters of the western Sargasso Sea crossing both tropical and subtropical waters as a major hurricane (i.e. at least category 3 (H3) on the Saffir-Simpson Hurricane Scale) from 31 August to 6 September (Fig. 1B). After the passage of Fabian two hurricanes crossed its trajectory, i.e. Hurricanes Isabel and Juan (Fig. 1B). The former crossed Fabian's trajectory in tropical waters on 14 September (approximately 10 days after the passage of

145 Fabian) (Beven & Cobb 2004) and the latter crossed Fabian's trajectory in subtropical waters
146 on 27 September (approximately three weeks after the passage of Fabian) (Avila 2012).
147 In general, Fabian moved over oligotrophic waters with a low Chl *a* concentration as observed
148 by satellite sensors (Fig. 1A). More specifically, it crossed the North Atlantic Subtropical Gyral
149 (West) and the North Atlantic Tropical Gyral biogeochemical provinces as defined by
150 Longhurst (1995) (Fig. 1B). These provinces have different oceanographic conditions in terms
151 of their ocean currents, fronts, and topography, which can lead to slightly different surface
152 Chl *a* concentration and depth-integrated production values (Longhurst 1995, 2007). The
153 North Atlantic Subtropical Gyral (West) is characterized by the presence of cold-core eddies
154 originating in the Gulf Stream meanders (Longhurst 2007). These eddies can import nutrients
155 into the euphotic zone fuelling phytoplankton production (Bibby et al. 2008). Moreover,
156 oceanic circulation in this province is influenced by the topography of the Mid-Atlantic Ridge
157 (Richardson 1985). Seamounts lead to enhanced surface Chl *a* concentration as they prompt
158 uplifting of isotherms and upwelling of nutrients (Longhurst 2007). In contrast, the North
159 Atlantic Tropical Gyral is characterized by a low surface current speed, a low eddy kinetic
160 energy (see Fig. 2c and d in Kuhn et al. 2019) and by low values of nutrient concentration and
161 phytoplankton biomass and productivity (Longhurst 2007). The regional pattern of
162 phytoplankton biomass appears to be dominated by the local effects of the deep nutricline
163 (Longhurst 2007). Fabian crossed the westernmost waters of the North Atlantic Tropical Gyral
164 province, which appear to be influenced by the oceanographic conditions of the adjacent
165 Caribbean province (Fig. 1B). This can explain the slightly higher Chl *a* concentration values
166 near the trajectory of Fabian in this area (Fig. 1A).
167 The ocean response to TC forcing varies between tropical and subtropical areas because of
168 different relationships between the TC transit speed and intensity with sea surface

temperature (SST), for instance (Mei et al. 2012, Mei & Pasquero 2013). Thus, in order to account for the different oceanographic conditions along Fabian's trajectory, as well as to account for potential different post-storm responses, we assessed the Fabian-induced oceanic response in the tropical and subtropical waters separately, considering the boundary between the North Atlantic Subtropical Gyral (West) and the North Atlantic Tropical Gyral biogeochemical provinces, i.e. at 25° N latitude approximately (Fig. 1B). We analysed the post-storm oceanic response along the part of Fabian's trajectory where it was a major hurricane (from 31 August to 6 September, Fig. 1B) to account for the strongest atmospheric forcing. For what concerns the vertical extent in the water column, we analysed the mean phytoplankton concentration in the euphotic zone (i.e. from the surface up to 200 m depth) as the main biological response variable in order to account for the post-storm stimulated growth of phytoplankton due to nutrient influx into the upper ocean. We assumed that phytoplankton growth below this zone cannot be substantially sustained because of sunlight limitation; hence, a post-storm phytoplankton concentration increase in the euphotic zone would not originate from biomass redistribution but from new phytoplankton production.

2.2. Modelled data

We used three-day composite data derived from the global configuration of the MIT marine ecosystem model (the 'Darwin Project' model) that are publicly available at the OPeNDAP server http://engaging-opendap.mit.edu:8080/las/UI.vm (last access: October 2021), dataset Darwin v0.2 cs510. The specific version of the model used to generate this dataset is described in Kuhn et al. (2019). In general, the biogeochemical and ecosystem components are governed by the MIT general circulation model (MITgcm) (Marshall et al. 1997). The latter uses the ECCO2 physical configuration with a horizontal resolution of 18 km and 50 depth levels, ranging from 10 m in the surface to 500 m at depth (Menemenlis et al. 2008, Kuhn et

al. 2019). At this horizontal resolution, the model captures mesoscale features such as eddies and fronts (Kuhn et al. 2019), which influence phytoplankton response to the passage of a TC (Chen & Tang 2012, Lü et al. 2020). The ecosystem model is based on Dutkiewicz et al. (2015) with parameterizations based on Ward et al. (2012) and includes a greater diversity as it resolves a total of 51 plankton types (35 phytoplankton grouped in 6 PFTs and 16 zooplankton) (Kuhn et al. 2019). Overall, the MIT marine ecosystem model simulates phytoplankton growth as a function of temperature, irradiance, and nutrients and includes zooplankton grazing (consult Dutkiewicz et al. 2015 for more details). Thus, phytoplankton abundance data account for both bottom-up and top-down controls on natural phytoplankton communities.

We assessed the post-storm response of the following PFTs: coccolithophores, diatoms, diazotrophs, mixotrophic dinoflagellates, picoeukaryotes, *Prochlorococcus* and *Synechococcus*. They differ in nutrient requirements, maximum growth rates, pigment composition, and palatability to grazers (Dutkiewicz et al. 2015, Kuhn et al. 2019). *Prochlorococcus* and *Synechococcus* are both picoprokaryotes but given their large ecotype and clade diversity (Zwirglmaier et al. 2008) have been considered as individual PFTs (e.g. Dutkiewicz et al. 2015). We investigated the *Prochlorococcus* and *Synechococcus* individual response as they are the dominant genera in our study area and in the oligotrophic ocean in general (Partensky et al. 1999a,b, Visintini et al. 2021).

Since TCs initiate a bottom-up forcing of the ecosystem (Fiedler et al. 2013), we mainly focused our analysis on the hurricane-induced changes on the phytoplankton community by bottom-up forcing, i.e. the phytoplankton response to nutrient increase. However, we briefly analysed the potential top-down effects on the post-storm phytoplankton bloom to better understand globally the biological response to the passage of Fabian. We considered the

mean nutrient concentration in the euphotic zone as the main abiotic driver of the post-storm response of the PFTs. This is supported by the fact that the TC-induced phytoplankton blooms are mainly attributed to the increased nutrient supply in the euphotic zone induced by vertical mixing (or entrainment) and upwelling during a TC (reviewed by Zhang et al. 2021). More specifically, it has been reported that nitrate availability tends to limit phytoplankton productivity in low-latitude oceans, including the North Atlantic Basin (Moore et al. 2008, 2013). Besides, certain phytoplankton groups have specific nutrient requirements. For instance, diatoms can be limited by silica (Boyd et al. 2010), while phosphate is relevant to coccolithophores (Thierstein & Young 2004, Mikaelyan et al. 2015). Thus, we used data of macronutrients: nitrate, phosphate and silica, as well as data of total zooplankton concentration (sum of 16 size classes) to address the possible top-down effects on the post-storm phytoplankton bloom.

Finally, we analysed data of the Shannon diversity index derived from this model to assess whether it captures coherent diversity changes in the phytoplankton community after the passage of Fabian. This index was computed as in Clayton et al. (2013), so by expressing the concentration of each phytoplankton type versus the total phytoplankton concentration in each grid cell, summed over the total number of phytoplankton types (i.e. 35 phytoplankton types as in Kuhn et al. 2019). The Shannon diversity index (*H*) is formally defined as:

$$H = -\sum_{i=1}^{S} p_i \ln(p_i), \quad (1)$$

where *s* is the total number of phytoplankton types and p_i is the relative concentration of type *i*. Although this index is computed on the basis of the phytoplankton type classification instead of the PFT classification, the latter accounts for all 35 phytoplankton types (i.e. 2 prokaryotes, 2 picoprokaryotes, 5 coccolithophores, 5 diazotrophs, 11 diatoms, 10

mixotrophic dinoflagellates) (Kuhn et al. 2019). Thus, post-storm changes in concentration of the analysed PFTs will be reflected in the values of the Shannon diversity index. In general, the term 'diversity' in this study reflects functional diversity, which is determined by the biogeochemical traits considered to define the PFTs (Dutkiewicz et al. 2015, 2020). The Shannon diversity index satisfies most of the axioms characterizing a diversity index (for more details, see Daly et al. 2018). Therefore, this index would allow to identify probable changes in phytoplankton diversity after the passage of a TC in oceanic waters, as illustrated in other studies for coastal waters (e.g. Mao et al. 2019, Baek et al. 2020).

2.3. Methodology and statistical analysis

The physical framework of a biogeochemical ocean general circulation model is fundamental to accurately simulate biogeochemical cycles and phytoplankton ecology in general (Clayton et al. 2017). Therefore, in order to confirm the suitability of the physical and ecosystem models to account for the oceanic response induced by Fabian, we performed a validation analysis. This allows to identify whether the post-storm oceanographic variability is reflecting the actual effects induced by Fabian or whether it originates from the limited model performance to account for such post-storm response. We compared the modelled SST and surface Chl *a* concentration (at 5 m depth) with satellite observations of these variables. Modelled Chl *a* concentration represents the total Chl *a* of 35 phytoplankton types; so, it accounts for the Chl *a* concentration of the whole phytoplankton community modelled. Natural phytoplankton communities are composed of a larger number of phytoplankton species and groups, which contribute to the Chl *a* concentration retrieved by satellite observations. Thus, when comparing modelled and satellite Chl *a* data, we focused on their patterns of temporal and spatial variability rather than the magnitude of this variable.

Daily SST data were derived from the Operational SST and Sea Ice Analysis (OSTIA) Reprocessed level 4 product (Donlon et al. 2012), provided by the Copernicus Marine Environment Monitoring Service at a spatial resolution of 0.05° x 0.05°. From this monitoring service, we also used the GlobColour multisatellite merged data of Chl *a* concentration (level 4 cloud free product), which is based on a spatial and temporal interpolation of the level 3 product at a spatial resolution of 0.0417° x 0.0417° (Garnesson et al. 2019a,b). The Chl *a* analyses involve multiple algorithms, i.e. the CI algorithm for oligotrophic waters (Hu et al. 2012) and the OC5 algorithm for mesotrophic and coastal waters (Gohin et al. 2002, Gohin, 2011).

Furthermore, we analysed modelled data of the mixed layer depth (MLD) to assess whether the physical model captures the storm-induced mixing in the study area. In general, quantitative validation of the vertical structure of the model was hampered because of the lack of suitable/extensive in situ datasets. Despite the availability of some observations (of physical variables mainly) from drifting buoys and floats of the Coupled Boundary Layer Air-Sea Transfer (CBLAST) Hurricane Program (Black et al. 2007) and the Bermuda Atlantic Time-series Study (BATS) site, these constitute point-based observations that neither match the horizontal (18 km) nor the vertical model resolution. Therefore, in order to qualitatively confirm the potential of the model to capture the oceanic post-storm response in the western Sargasso Sea, we compared our results with those previously reported in literature under similar conditions. This approach circumvents the lack of suitable/extensive in situ datasets, as well as the limitations of the satellite-based PFT algorithms to generate accurate estimates to validate the model outputs.

We built times series of the three-day composite data derived from the MIT marine ecosystem model. In view of the low temporal resolution of these modelled data and in order

286 to increase the number of observations to better distinguish temporal dynamics, we analysed
287 data of August (before Fabian), September (during and after Fabian) and October (after
288 Fabian). As satellite observations of SST and Chl *a* concentration have a daily resolution, we
289 computed three-day composite satellite data matching the dates of the modelled ones in
290 order to compare these datasets at the same temporal resolution.
291 In previous studies assessing the post-storm oceanic response in the western North Atlantic
292 Basin, authors used 200 km radius disks centered at the consecutive TC positions (e.g.
293 Shropshire et al. 2016). This radius aligns with the average storm size in the North Atlantic
294 (Kimball & Mulekar 2004). On the other hand, Kuhn et al. (2019) reported that autocorrelation
295 up to 100 km occurs for PFT concentrations in subtropical oligotrophic regions, indicating that
296 phytoplankton assemblages up to 100 km apart respond similarly to oceanographic
297 variability. For that reason, we assessed the response of the PFTs along the trajectory of
298 Fabian in both 200 and 100 km radius disks centered at consecutive hurricane positions (see
299 Fig. 1C for a representation of the 100 km radius disks centered at hurricane positions). In
300 both cases, we found a similar temporal evolution of the post-storm phytoplankton
301 concentration. Hence, we show the times series of all studied variables derived from 100 km
302 radius disks as they account for the highest values of these variables, allowing to clearly
303 observe specific temporal responses. Overall, the mean values of the consecutive disks were
304 averaged to retrieve the mean response along Fabian's trajectory in the tropical and
305 subtropical waters separately, in agreement with the methodology outlined by Babin et al.
306 (2004).
307 We used a dependent sample t-test at 0.05 significance level (after confirming normality
308 according to Kolmogorov-Smirnov and Shapiro-Wilk tests) to compare the concentrations of
309 the PFTs and nutrients, as well as the values of the Shannon diversity index in August and

September, in order to account for the Fabian-induced oceanographic variability over its entire trajectory. This test is suitable to compare two groups of scores and their means when assessing pre- and post-conditions to a given event (Gerald 2018). In general, the passage of a TC disrupts the seasonal cycle of the analysed oceanographic variables. Hence, when comparing their pre- and post-storm means we are mainly accounting for the variability induced by this event in particular.

3. RESULTS

3.1. Validation of the physical and the ecosystem models

From Fig. 2A, we observe that both modelled and satellite SSTs followed a similar temporal variability along Fabian's trajectory in the tropical waters. Modelled data underestimate satellite observations by 0.7, 0.3 and 0.6% in August, September and October, respectively. In contrast, the largest differences between modelled and satellite SST values in the subtropical waters occurred in August, prior to the passage of Fabian (Fig. 2B) when modelled data underestimate satellite observations by 2.5%.

When analysing the spatially explicit SST response in Fig. 3, we can see that, indeed, the physical model captures the regional patterns of SST as well as the post-storm cooling induced by Fabian. The latter could imply that the physical model accounts for the storm-induced vertical mixing, which mainly drives the post-storm surface cooling (Price 1981). Vertical mixing and the associated deepening of the mixed layer is also the primary mechanism through which nutrients are brought to the ocean surface in the oligotrophic North Atlantic after the passage of TCs (Foltz et al. 2015). Figure 2C shows that Fabian led to a mean deepening of the MLD of approximately 5 m along its tropical trajectory, while no response was observed along its subtropical trajectory (Fig. 2D). The former result largely agrees with the findings of Foltz et al. (2015) as they reported that the spatially averaged MLD derived

334 from HYCOM simulations increases by 7 m after the passage of TCs in the western Sargasso
335 Sea in the period 2008–2013. In contrast, the lack of response along the subtropical trajectory
336 of Fabian disagrees with the findings of Son et al. (2007) and Black & Dickey (2008). They
337 reported a substantial deepening of the MLD after the passage of Fabian in the subtropical
338 Sargasso Sea, leading to a significant satellite surface Chl *a* concentration increase via upper
339 ocean nutrient enrichment. The physical model assimilates satellite data of SST (Menemenlis
340 et al. 2008), leading to consistent estimates of this variable in both study areas (Fig. 3).
341 However, the model seems unable to capture the deepening of the MLD induced by Fabian
342 in the subtropical waters.
343 For what concerns the surface Chl *a* concentration, we found that the modelled spatially
344 averaged data along the entire tropical and subtropical trajectory did not properly capture
345 the immediate response to the passage of Fabian as observed remotely (Fig. 4A and B). The
346 model simulated a Chl *a* concentration increase at three-day composite 15 (Fig. 4A), which
347 was associated with the long-lasting effects induced by Fabian, as well as the effects induced
348 by Isabel, which crossed the tropical trajectory of Fabian on 14 September (at the intersection
349 of three-day composites 15 and 16) (Fig. 1B). This increased Chl *a* concentration is largely
350 consistent with the deepening of the MLD observed in Fig. 2C. In order to analyse the
351 modelled and satellite Chl *a* concentration in a spatially explicit way, we computed anomalies.
352 They allow to better observe the post-storm response due to the highly uneven spatial
353 distribution of the Chl *a* concentration in the study area. Thus, we subtracted the mean value
354 of the three-day composites 9 and 10 (which largely account for the pre-storm week) from
355 the post-storm three-day composites 12, 13 and 16. The first two post-storm composites
356 account for the passage of Fabian over the entire tropical and subtropical areas, respectively,
357 while the latter accounts for the passage of Isabel across the tropical waters. When analysing

358 local responses of Chl *a* concentration along the tropical trajectory of Fabian, we found that
359 the time series of modelled and satellite Chl *a* concentration followed a similar temporal
360 evolution in the area delineated by the disk in Fig. 5. In this area, modelled data accounted
361 for both the Chl *a* concentration increase induced by Fabian and the one induced by Isabel
362 (Figs. 4C and 5). The temporal variability of the modelled Chl *a* concentration time series was
363 also consistent with the one of the MLD (Fig. 4D). This local increase of Chl *a* concentration
364 was the highest one occurring in the tropical waters during our study period (Fig. 5).
365 From this validation analysis, we conclude that the ecosystem model captures the largest and
366 most spatially extended surface Chl *a* concentration responses in the tropical waters.
367 Although the strongest mixing induced by hurricanes (driving the upward transport of
368 nutrients) occurs at the ocean surface, the TC-induced nutrient increase is higher deep in the
369 euphotic zone than at the ocean surface as nutrient concentration increases with depth
370 (Boyer et al. 2006, Zhao et al. 2008). Thus, we might expect that the strongest PFT response
371 to nutrient enrichment simulated by the model occurs deep in the euphotic zone (assuming
372 an optimal intensity of sunlight). We verify this hypothesis in Section 3.2 by analysing profiles
373 of the PFTs and nutrient concentration.
374 On the other hand, the passage of Fabian across the subtropical waters appears to have led
375 to positive anomalies of the modelled Chl *a* concentration to the right side of its trajectory
376 (Fig. 5B and C). However, modelled Chl *a* concentration anomalies above 25° N latitude are
377 distributed heterogeneously as compared with satellite observations (Fig. 5). Consequently,
378 spatially averaged data within the disks along Fabian's trajectory did not resolve a net Chl *a*
379 concentration increase, even using the smallest radius (100 km) reported in the literature to
380 account for spatial autocorrelation of PFTs (Kuhn et al. 2019). Our findings are consistent with
381 the ones reported by Kuhn et al. (2019). They found that, at climatological scale, the

coefficient of variation of the modelled Chl *a* concentration in the subtropical western North Atlantic is higher than that computed from satellite observations and also higher than that in the tropical North Atlantic (see Fig. S2 in Kuhn et al. 2019). Despite the different responses observed in the tropical and subtropical waters, in the following section, we present the results for both areas in order to confirm the conclusions derived from our validation analysis.

3.2. Phytoplankton concentration and diversity

Fabian induced a significant concentration increase (t-test, $p < 0.05$) of all analysed PFTs in tropical waters, except for *Prochlorococcus* (Fig. 6, left panel). The increased post-storm phytoplankton concentration persisted the entire post-storm month of September, and started to decrease in October. In general, the concentrations of coccolithophores, diatoms, diazotrophs, mixotrophic dinoflagellates, picoeukaryotes, *Prochlorococcus* and *Synechococcus* in tropical waters were 17, 20, 8, 21, 9, 1 and 2.6% higher in September as compared to August. In contrast, we did not find such a clear pattern in the subtropical waters, where phytoplankton concentration decreased gradually from August on (Fig. 6, right panel). Only coccolitophores and diatoms showed a limited (t-test, $p > 0.05$) concentration increase approximately six days after the passage of Fabian (Fig. 6B and D). Overall, in both tropical and subtropical waters, the post-storm variability of phytoplankton concentration did not change significantly (t-test, $p > 0.05$) the contribution of each PFT to the total phytoplankton concentration (Fig. 7).

When analysing the nutrient concentrations, we found a significant increase (t-test, $p < 0.05$) of nitrate, phosphate and silica after the passage of Fabian across the tropical waters (Fig. 8, left panel). This post-storm response was largely consistent with the one shown by the PFTs in September in this area (Fig. 6, left panel). Subsequently, in October, the concentrations of nutrients remained high although those of phytoplankton decreased (Figs. 6 and 8, left

406 panels). In contrast, the nutrient concentrations in the subtropical waters did not respond
407 considerably to the passage of Fabian (Fig. 8, right panel). Although the nutrient
408 concentrations along the tropical trajectory had a distinct temporal dynamics during the
409 passage of the hurricane, they overestimate in situ observations in both study areas. Near-
410 complete depletion of nitrate usually occurs in the upper 100 m of the tropical and subtropical
411 Sargasso Sea (i.e. below its limit of detection 0.03 mmol m^{-3}, Moore et al. 2008, 2013). More
412 specifically, observations at the BATS site before the passage of Fabian indicate that combined
413 nitrate and nitrite concentrations increased from undetectable levels at 100 m to 2.6 mmol
414 m^{-3} at 200 m (Black & Dickey 2008).
415 Considering the phosphate concentration values in Fig. 8C and D, and assuming a Redfield
416 NO_3:PO_4 ratio of 16:1 (Redfield 1958), nitrate concentrations should be in the range of 0.29–
417 0.45 and 0.65–0.88 mmol m^{-3} in the tropical and subtropical waters, respectively, during the
418 entire study period. These adjusted nitrate concentrations are largely consistent with the
419 observations. For instance, the adjusted mean nitrate in the euphotic zone in September
420 along the tropical (subtropical) trajectory of Fabian is 0.43 (0.80) mmol m^{-3}, while the
421 climatological mean value of this variable from the World Ocean Atlas (Boyer et al. 2018) is
422 0.49 (0.89) mmol m^{-3} (results not shown). Even though nitrate concentrations of the Darwin
423 v0.2 cs510 overestimate field observations, we still analysed these data in order to confirm
424 that the model captures the spatiotemporal dynamics of nitrate to the passage of Fabian
425 properly.
426 Although we did not assess quantitatively the post-storm causal relationship between the PFT
427 and the nutrient concentrations, the consistent temporal variability of the time series of these
428 variables in the tropical waters can give insights into the effects of nutrients modulating the
429 immediate post-storm phytoplankton response. In order to qualitatively confirm whether the

model captures this causal relationship, we analysed time series in two areas that were not affected by hurricanes (disks 1 and 3 in Fig. 1C) and in an area affected by Hurricane Isabel in the tropical waters (disk 2 in Fig. 1C). Since the time series derived from the former two disks are similar, we only display the ones from disk 1. Figure 9A and B display the time series of diatom and mixotrophic dinoflagellate concentrations as they showed the maximum concentration increases to the passage of Fabian, indicating they are sensitive to nutrient changes.

Overall, the patterns of temporal variability of the phytoplankton concentrations in disks 1, 2 and 3 largely match those of nutrients, suggesting that the model captures the effect of nutrients on phytoplankton communities in this oligotrophic area. However, in October, we found peculiar responses. For instance, in the areas that were not affected by hurricanes (disks 1 and 3), phytoplankton concentration increases were not significant as compared with the ones of the nutrient concentration at this time (Fig. 9, left panel). On the other hand, we observe that, in the area affected by Isabel (disk 2), phytoplankton concentration started to decrease from the beginning of October on when the nutrient concentrations were still high (Fig. 9, right panel). The high nutrient concentrations in October could be associated with a seasonal cycle of this variable in the tropical western Sargasso Sea. The fact that the high nutrient concentrations at this time did not substantially influence the phytoplankton concentration indicate that other environmental factors (probably including top-down controls of phytoplankton blooms) are constraining the phytoplankton response. More studies are needed to unravel the relationship between the nutrient and the PFT concentrations in October.

In order to better assess the post-storm response of the PFTs captured by the model in the tropical western Sargasso Sea, we computed profiles before and after the passage of Fabian.

Pre-storm profiles account for the mean concentration of three-day composites 9 and 10, which largely account for the pre-storm week conditions and post-storm profiles account for the mean concentration of three-day composites 11, 12, 13, 14 and 15, which largely account for the two post-storm week conditions. This is supported by the fact that the strongest TC-induced phytoplankton response as inferred from Chl *a* satellite observations is observed between two to three weeks after the passage of TCs (Babin et al. 2004, Menkes et al. 2016). Figure 10 (upper panel) shows that the model does not capture any meaningful post-storm perturbation of the PFT concentration in the first 100 m of the water column along the tropical trajectory of Fabian. The post-storm concentration increases are mainly observed between 100–175 m depth across all PFTs (Fig. 10, upper panel), which are associated with the high nutrient concentration increases at these depths (Fig. 11, upper panel). This result confirms that the model captures the causal relationship between nutrient and PFT concentration increases in the tropical waters in general, and the largest phytoplankton responses to the passage of Fabian in particular.

On the other hand, in Fig. 10 (upper panel), we observe that the maximum concentration of each PFT was reached at variable depths in the tropical euphotic zone. We refer to this maximum phytoplankton concentration as the deep biomass maximum (DBM). In most cases, the post-storm concentration increases occurred in the waters above the depth of the pre-storm DBM (Fig. 10, upper panel). Then, from the depth of maximum concentration on, there was a concentration decrease as compared with the pre-storm values. In contrast, we did not observe a considerable variability of the vertical profiles of the nutrient and PFT concentrations in the subtropical waters due to the passage of Fabian (Fig. 10, bottom panel). The latter disagrees with observations as Fabian led to an increased primary production and

phytoplankton pigment concentration in the first 100 m of the water column in the waters surrounding Bermuda (see Fig. S3b in Pedrosa-Pàmies et al. 2019).

Up to this point, we have assessed the effects of nutrients influencing the PFT responses. However, the analysis of both bottom-up and top-down effects is necessary in order to better understand the dynamics of the post-storm phytoplankton blooms. Figure 12 shows the time series of total phytoplankton (sum of the 7 PFTs) and zooplankton concentrations. In general, both communities showed coupled dynamics in August and October and a decoupled one in September in the tropical waters probably because of the perturbations induced by Fabian (Fig. 12A and C). In contrast, no post-storm responses were observed in the subtropical waters (Fig. 12B and D). Fabian induced a slight increase of the zooplankton concentrations following its passage at the beginning of September (grey-shaded area in Fig. 12C) as compared with the phytoplankton increase at this time (grey-shaded area in Fig. 12A). Then, once Fabian left the study area (from three-day composite 13 on) the phytoplankton concentrations increased progressively until the end of September (Fig. 12A), whereas the zooplankton concentrations remained quite stable during this period (Fig. 12C). The former indicates the existence of suitable environmental conditions that stimulated the phytoplankton community growth after the passage of Fabian, e.g. increased nutrient supply (Fig. 8A, C) as well as limited grazing pressure because of the decoupled predator-prey interaction (Fig. 12A and C).

Finally, for what concerns the effects of Fabian on phytoplankton diversity, we found a significant (t-test, $p < 0.05$) post-storm increase of the Shannon diversity index values in the tropical waters (Fig. 13A). In those waters, its monthly mean value was 5% higher in September than in August, while this was only 0.7% in the subtropical waters. Although the Shannon diversity was high in September and October in the tropical waters compared with

August, it showed a slightly decreasing trend after the passage of Fabian. This could indicate a weakening of the Fabian-induced effects on diversity.

4. DISCUSSION

In this study, we assessed the potential of the MIT marine ecosystem model to capture the post-storm response of PFTs to the passage of Fabian in the western Sargasso Sea by analysing the Darwin v0.2 cs510 dataset. Taking into account the findings presented in Section 3 regarding the lack of oceanographic variability in the subtropical waters after the passage of Fabian, we suggest that this is determined by model shortcomings rather than by the actual lack of a post-storm response in this area. Therefore, we mainly focus our discussion on the response observed in the tropical waters. In Section 4.3, we briefly address the general model shortcomings, though a detailed discussion thereof is not feasible as we analysed publicly available model outputs without executing the model. Overall, this exploratory study aims to stimulate and guide future modelling efforts to improve model performance and generate new knowledge on the post-storm phytoplankton community response.

4.1. Phytoplankton concentration

In general, the increased phytoplankton concentration after the passage of Fabian across the tropical waters was associated with the increase of nutrients in this oligotrophic region (Figs. 6 and 8). Post-storm blooms of coccolithophores have been observed for more than a month in the Black Sea due to the continuous entrainment of nitrate and phosphate into the euphotic layer (Stanichny et al. 2021). During the relaxation stage (i.e. when the TC leaves the study area), upwelling of nutrient-rich waters can occur in the western Sargasso Sea (Avila-Alonso et al. 2021), leading to a continuous supply of nutrients into the euphotic zone. Therefore, the increased post-storm nutrient concentrations during September suggest that the model accounts for the physical oceanographic variability induced by Fabian modulating

524 the fluxes of nutrient in the deep euphotic zone mainly. On the other hand, the maximum
525 concentration increase of diatoms and mixotrophic dinoflagellates (i.e. 20 and 21%) found in
526 this study is consistent with the fact that the microplanktonic fraction (diatoms and
527 dinoflagellates) is typically the one showing the strongest response to storm-induced nutrient
528 enrichment (Platt et al. 2005, Son et al. 2007, Mangesh et al. 2016, Painter et al. 2016, Mao
529 et al. 2019).
530 The post-storm nutrient enrichment simulated by the model does not equally impact all PFTs,
531 since we found a weak concentration increase of *Prochlorococcus* after the passage of Fabian
532 across the tropical waters (Fig. 6K). Besides, the contribution of *Prochlorococcus* to the total
533 phytoplankton concentration decreased by at most 8% in the tropical waters in September.
534 These results agree with field observations. For instance, Painter et al. (2016) reported a
535 considerable decrease of the picoplankton (<2 µm, cyanobacteria including *Prochlorococcus*)
536 contribution to the phytoplanktonic community after the passage of an intense autumn storm
537 through the temperate northeast Atlantic. *Prochlorococcus* numerically dominate
538 phytoplankton communities in oligotrophic oceans mainly because of its tiny cell size (0.5–
539 0.8 µm, reviewed by Bertilsson et al. 2003), and the resulting high surface-to-volume ratio
540 that provides adaptative advantages for nutrient uptake (Chisholm 1992, Partensky et al.
541 1999b). It has been reported that deep mixing, which drives nutrient fluxes into the euphotic
542 zone near Bermuda, leads to a significantly lower abundance of *Prochlorococcus* than during
543 the stratified, nutrient-poor conditions (DuRand et al. 2001). Overall, our findings suggest that
544 the model is able to simulates the weak effect of nutrient enrichment on *Prochlorococcus* as
545 compared with other PFTs.
546 On the other hand, the profile analysis revealed that the model reproduces patterns of
547 vertical variability reported in literature. For instance, the increased (decreased) post-storm

548 phytoplankton concentration in the waters above (below) the DBM (Fig. 10, upper panel)
549 agrees with the vertical variability of the Chl *a* concentration reported after the passage of
550 Hurricane Dorian (2019) across the western Sargasso Sea (Avila-Alonso et al. 2021). Although
551 the deep chlorophyll maximum (DCM) does not always coincide with biomass or productivity
552 maxima, it often corresponds to peaks in abundance of phytoplankton (reviewed by Moeller
553 et al., 2019). Thus, we might consider the Chl *a* concentration in the DCM as a proxy of
554 phytoplankton abundance. Overall, the post-storm nutrient enrichment induced by Fabian
555 fuelled phytoplankton growth above the DBM (Figs. 10 and 11, upper panel) as observed by
556 Avila-Alonso et al. (2021). Then, the increased phytoplankton concentration in the shallower
557 waters can moderately limit deep photosynthesis because of the sunlight attenuation.
558 Moreover, the relative depth where the PFTs reached their maximum concentration was
559 consistent with observations (e.g. Latasa et al. 2016, 2017, Kang et al. 2021). More specifically,
560 Latasa et al. (2017) reported that within the DCM layer *Prochlorococcus* and *Synechococcus*
561 preferred shallow waters, while diatoms and coccolithophores preferred deep layers.
562 *Prochlorococcus* and *Synechococcus* can reach maximum concentrations above the nutrient-
563 rich deep waters because they can cope with low nutrient conditions (Partensky et al.
564 1999a,b). More specifically, for the case of *Synechococcus*, it was suggested that they can
565 sacrifice nutrient needs (which are higher than the ones of *Prochlorococcus*) in order to
566 improve the light field and optimize growth (Latasa et al. 2016). In contrast, diatoms can
567 dominate deeper than optimal irradiance layers, probably to meet their high nutrient
568 requirements (Latasa et al. 2016, 2017). Kang et al. (2021) found that diatoms were the most
569 abundant PFT at the base of the euphotic zone (1% surface irradiance) during summer in the
570 oligotrophic Yellow Sea and East China Sea with nutrient concentration being the major factor
571 controlling this vertical distribution. Besides, although coccolithophores show a variable

572 vertical distribution in the warm tropical and subtropical waters, they can be found in the
573 lower euphotic zone (10–1% surface irradiance) close to the nutricline (Poulton et al. 2017).
574 Despite the consistent variability of the relative depths of the DBM across all PFTs, the actual
575 depths where these maxima occur are deeper than observations. For instance, the mean
576 depth of the DCM in the oceanic basins at 20° and 30° N is approximately 84 and 92 m,
577 respectively (Cornec et al. 2021), while the DCM layer at the BATS site typically occurs
578 between 60 and 120 m (Steinberg et al., 2001). The enhanced post-storm phytoplankton
579 response deep in the euphotic zone appears to have been driven by the high nutrient
580 concentration increases in these waters (Figs. 10 and 11, upper panel). Still, it has been
581 reported that the appearance and depth of DCMs globally are primarily driven by sunlight
582 attenuation (Cornec et al. 2021). The model resolves the penetration of spectral irradiance as
583 it is absorbed and scattered within the water column by the water constituents including
584 phytoplankton (Dutkiewicz et al. 2015). The low phytoplankton concentrations simulated by
585 the model in the upper ocean (Fig. 10, upper panel) do not contribute considerably to sunlight
586 attenuation. Consequently, high irradiance doses can reach the deep and nutrient-rich waters
587 in the euphotic zone supporting photosynthesis. Thus, in order to simulate the DBMs at
588 shallower depths, the model should be able to capture the moderate phytoplankton response
589 in the upper ocean after the passage of TCs.
590 For what concerns the potential top-down effects on the post-storm phytoplankton bloom,
591 we found that Fabian seems to have induced a decoupled predator-prey interaction in the
592 tropical waters (Fig. 12A and C). The storm-induced mixing and turbulence can decrease
593 phytoplankton losses due to zooplankton grazing as mixing dilutes their abundance and
594 reduces their encounter rates (Morison et al. 2019). Deep mixing allows phytoplankton to
595 escape from grazers leading to phytoplankton biomass accumulation in the euphotic zone as

596 the phytoplankton growth rate surpasses that of zooplankton grazing (Morison et al. 2019).
597 Then, once the physical disturbance ends (e.g. the storm-induced mixing and turbulence), the
598 increased phytoplankton concentration enhances the encounter rate between phytoplankton
599 and their predators, thereby reinforcing predator populations and intensifying density-
600 dependent losses (Behrenfeld 2014).
601 Zooplankton grazing is simulated using a Holling III scheme (Dutkiewicz et al. 2015). This
602 functional response is described by a sigmoidal curve indicating that at high levels of prey
603 density, a saturation of the number of prey consumed for predator occurs because of the time
604 required for predators to digest each captured prey (Holling 1959, Rohr et al. 2022). Thus,
605 the high phytoplankton concentration induced by Fabian via nutrient enrichment could
606 ultimately have enhanced the encounter rate between phytoplankton and zooplankton,
607 leading to a saturation of the zooplankton grazing rate and consequently to a limited biomass
608 increase during September (Fig. 12C). From this analysis, we conclude that although the post-
609 storm phytoplankton bloom appears to be supported by both the nutrient supply and the
610 limited grazing pressure, the former plays a major role in initiating and fuelling the post-storm
611 phytoplankton bloom.

612 **4.2. Phytoplankton diversity**

613 Given our analysis of the mean phytoplankton concentration in the euphotic zone, we
614 consider that the post-storm concentration increase can be associated with new
615 phytoplankton production and not with the supply of phytoplankton cells from below the
616 euphotic zone. A clear relationship between productivity and diversity in marine
617 phytoplankton communities has been established before (e.g. Irigoien et al. 2004, Vallina et
618 al. 2014). These authors found that, at global scale, diversity increases linearly with primary

619 production at low production regimes, reflecting the resource supply into the ecosystem.
620 Moreover, it has been suggested that nutrient supply may be the key regulator of diversity in
621 the very oligotrophic waters surrounding the BATS area (Pinckney & Richardson 2016).
622 Thus, the post-storm increased nutrient concentration simulated by the model not only
623 caused an increased phytoplankton concentration but it also affected diversity. Apparently,
624 the limited increase of the share of fast-growing phytoplankton groups such as diatoms and
625 coccolithophores and decrease of the proportion of dominant groups that grow under strong
626 nutrient limitation conditions (i.e. picoeukaryotes, *Prochlorococcus* and *Synechococcus*)
627 impacted the diversity of the phytoplankton community in the tropical waters (Figs. 7 and
628 13A). Then, in October, the contribution of *Prochlorococcus* increased, while that of diatoms
629 decreased compared with their contributions in September (Fig. 7). These slight variations
630 appear to have affected the phytoplankton community diversity leading to the observed
631 decreasing trend at this time (Fig. 13A).
632 In contrast, a decrease of phytoplankton Shannon diversity after the passage of TCs across
633 coastal waters has been observed as a result of a post-storm dominance of diatoms due to
634 large nutrient supply (Baek et al. 2020). In general, a decrease of phytoplankton diversity
635 occurs at a high nutrient supply because a few fast-growing opportunistic (e.g. diatoms) can
636 grow almost uncontrolled in absence of predators, leading to high primary productivity
637 (Irigoien et al. 2004, Vallina et al. 2014). Thus, we suggest that a moderate post-storm nutrient
638 increase in oligotrophic tropical waters appears to positively impact phytoplankton diversity,
639 by limiting productivity of opportunistic groups and decreasing the share of dominant groups.
640 These slight changes lead to a post-storm phytoplankton community a little bit more evenly
641 distributed than the undisturbed community before the passage of Fabian. From this

642 discussion, we conclude that the modelled post-storm phytoplankton diversity response was
643 consistent with the general knowledge on the topic.

644 **4.3. Model limitations and future work**

645 From this exploratory study, we demonstrated that the MIT marine ecosystem model
646 simulates the largest TC-induced changes in nutrient, Chl *a* and PFT concentrations as well as
647 changes in phytoplankton diversity in the tropical western Sargasso Sea. However, it fails to
648 capture the moderate responses in the upper ocean. Although the horizontal resolution of
649 the model captures mesoscale features such as eddies and fronts, TCs affect the physical
650 ocean dynamics and the phytoplankton productivity at submesoscale (Smith et al. 2019, Whitt
651 et al. 2019). The Darwin v0.2 cs510 dataset analysed here is derived from the global
652 configuration of the MIT marine ecosystem model. However, a high-resolution regional model
653 might be able to resolve moderate and/or more local phytoplankton post-storm responses in
654 the upper ocean layer. Besides, future research should consider a higher temporal resolution
655 to observe the immediate impacts of storms on the different PFTs that may respond over
656 different time scales (Painter et al. 2016).

657 Even though the results presented here give insights into the effects of nutrients modulating
658 the immediate post-storm phytoplankton response in the tropical western Sargasso Sea,
659 future modelling studies might assess the strength of the causal relationship between
660 individual PFTs and nutrient species through a controlled experiment (e.g. a model sensitivity
661 analysis). This type of study would allow to quantitatively assess the response of each PFT to
662 variable nutrient conditions after the passage of TCs. Besides, although it has been reported
663 that the model captures the global patterns in macronutrients seen in the compilation of in
664 situ observation from the World Ocean Atlas (Dutkiewicz et al. 2015), a model examination is

665 needed in order to adjust the modelled nitrate estimates of the Darwin v0.2 cs510 dataset
666 with observations in the western North Atlantic.
667 On the other hand, given the coherent temporal evolution of the total phytoplankton and
668 zooplankton concentrations in the tropical waters (Fig. 12A and C), we consider that the
669 model properly captures the trophic interactions between these groups of organisms after
670 the passage of Fabian. Overall, the analysis of the possible top-down effects presented here
671 merely aims to serve as a motivation for a more extensive future analysis supported by field
672 observations and considering the zooplankton grazing preferences influencing individual PFT
673 responses.
674 For what concerns the lack of response along the subtropical trajectory after the passage of
675 Fabian, we consider that this is determined by model shortcomings (e.g. inability to simulate
676 the deepening of the MLD) rather than by the actual lack of a post-storm response in this
677 area, as we mentioned before. The subtropical western North Atlantic is affected by the
678 eastward extension of the Gulf Stream, which contributes to the formation and shedding of
679 eddies in the region (Kang & Curchitser 2013), leading to a considerable spatial heterogeneity.
680 Thus, future research needs to be focused on the assessment and improvement of the model
681 performance in this oceanographically complex area. Besides, although ECCO2 considers wind
682 stress forcing from meteorological reanalysis data (Menemenlis et al. 2005), an improved
683 atmospheric forcing using TC winds from the Hurricane Database (HURDAT) of the National
684 Hurricane Center (http://www.aoml.noaa.gov/hrd/hurdat/hurdat2.html), for instance, might
685 allow to more accurately simulate post-storm responses in both study areas.
686 Finally, we acknowledge that a full assessment of the TC-induced PFT variability needs to be
687 supported by in situ data because of the numerous complex effects in the phytoplankton
688 community that cannot be resolved easily by alternative data sources (Painter et al. 2016).

Besides, extensive in situ datasets are required for model validation. Thus, improved and expanded ocean sensor capabilities including both traditional observation methods, such as buoys and moorings, air-deployed drifters and floats, Argo floats, as well as more advanced observation technology and methods such as gliders and wave gliders (reviewed by Zhang et al. 2021) are necessary to support future modelling studies.

5. CONCLUSIONS

This is the first study assessing the potential of the MIT marine ecosystem model to describe the response of PFTs to the passage of a hurricane in the western Sargasso Sea. The analysis of modelled data showed that Hurricane Fabian induced a significant mean concentration increase (t-test, $p < 0.05$) of the analysed PFTs in the tropical euphotic zone, except for *Prochlorococcus*. Although this biological response was driven by both the mean concentration increase of nitrate, phosphate and silica in the euphotic zone to the passage of Fabian and by a limited zooplankton grazing pressure, the former plays a major role in initiating and fuelling the post-storm phytoplankton bloom. Besides, a significant increase of the Shannon diversity index values was observed. Changes in diversity in this area appear to have been associated with the post-storm nutrient enrichment, which stimulated growth of fast-growing PFTs (e.g. diatoms and coccolithophores) and decreased the contribution of slow-growing dominant groups (e.g. picoeukaryotes, *Prochlorococcus* and *Synechococcus*) to the phytoplanktonic community. In general, this model captured the causal relationship between nutrient and PFT concentration increases in the tropical waters, which is a prerequisite to assess the post-storm biological oceanic response. More specifically, the model captured the largest PFT responses such as those in the deep euphotic zone, whereas it was unable to mimic the moderated ones in the upper ocean. On the other hand, a clear biological response to the passage of Fabian across the subtropical waters was not discerned.

The model did not appropriately capture the oceanic perturbations induced by Fabian as observed in satellite imagery in the subtropical waters. The subtropical western Sargasso Sea is a very complex oceanographic area influenced by the Gulf Stream eastward extension zone, which appears to constrain the model performance to account for extreme environmental conditions induced by a hurricane. The results presented in this work can stimulate and guide both modelling studies aiming to improve model performance and field studies, which are fundamental to collect data and generate accurate knowledge needed for model validation.

ACKNOWLEDGMENTS

We are grateful to Mick Follows and Oliver Jahn from the Massachusetts Institute of Technology for generously helping us to get the data of the MIT marine ecosystem model as well as for kindly addressing all our queries.

COMPETING INTERESTS

The authors declare that they have no known competing financial interests or personal relationships that could have appeared to influence the work reported in this paper.

AUTHOR CONTRIBUTIONS

All authors together have contributed to the research reported in different ways. Dailé Avila-Alonso: Conceptualization, Data curation, Formal analysis, Visualization, Roles/Writing - original draft; Jan M. Baetens: Conceptualization, Methodology, Writing - review and editing; Rolando Cardenas: Formal analysis, Methodology; Bernard De Baets: Supervision, Funding acquisition, Writing - review and editing.

FINANCIAL SUPPORT

This research has been supported by the Special Research Fund (BOF) of Ghent University, Belgium (grant no. 01W03715).

REFERENCES

737 Anglès S, Jordi A, Campbell L (2015) Responses of the coastal phytoplankton community to
738 tropical cyclones revealed by high-frequency imaging flow cytometry. Limnology and
739 Oceanography 60:1562–1576
740 Avila L (2012) Tropical Cyclone Report Hurricane Juan, 24–29 September, 2003. National
741 Hurricane Center, https://www.nhc.noaa.gov/data/tcr
742 Avila-Alonso D, Baetens JM, Cardenas R, De Baets B (2021) Oceanic response to the
743 consecutive Hurricanes Dorian and Humberto (2019) in the Sargasso Sea. Natural
744 Hazards and Earth System Sciences 21:837–859
745 Babin SM, Carton JA, Dickey TD, Wiggert JD (2004) Satellite evidence of hurricane-induced
746 phytoplankton blooms in an oceanic desert. Journal of Geophysical Research: Oceans
747 109: C03043. https://doi.org/10.1029/2003JC001938
748 Baek SH, Lee M, Park BS, Lim YK (2020) Variation in phytoplankton community due to an
749 autumn typhoon and winter water turbulence in southern Korean coastal waters.
750 Sustainability 12:2781. https://doi.org/10.3390/su12072781
751 Behrenfeld MJ (2014) Climate-mediated dance of the plankton. Nature Climate Change
752 4:880–887
753 Bertilsson S, Berglund O, Karl DM, Chisholm SW (2003) Elemental composition of marine
754 *Prochlorococcus* and *Synechococcus*: implications for the ecological stoichiometry of the
755 sea. Limnology and Oceanography 48:1721–1731
756 Beven J, Cobb H (2004) Tropical Cyclone Report Hurricane Isabel, 6–19 September 2003.
757 National Hurricane Center, https://www.nhc.noaa.gov/data/tcr
758 Bibby T, Gorbunov M, Wyman K, Falkowski P (2008) Photosynthetic community responses to
759 upwelling in mesoscale eddies in the subtropical North Atlantic and Pacific Oceans.
760 Deep Sea Research Part II 55:1310–1320

761 Black WJ, Dickey TD (2008) Observations and analyses of upper ocean responses to tropical
762 storms and hurricanes in the vicinity of Bermuda. Journal of Geophysical Research:
763 Oceans 113:C08009. https://doi.org/10.1029/2007JC004358
764 Black PG, D'Asaro EA, Drennan WM, French JR, Niiler PP, Sanford TB, Terrill EJ, Walsh EJ, Zhang
765 JA (2007) Air-sea exchange in hurricanes: synthesis of observations from the Coupled
766 Boundary Layer Air-Sea Transfer experiment. Bulletin of the American Meteorological
767 Society 88:357–384
768 Bonachela JA, Klausmeier CA, Edwards KF, Litchman E, Levin SA (2016) The role of
769 phytoplankton diversity in the emergent oceanic stoichiometry. Journal of Plankton
770 Research 38:1021–1035
771 Boyd PW, Strzepek R, Fu F, Hutchins DA (2010) Environmental control of open-ocean
772 phytoplankton groups: now and in the future. Limnology and Oceanography 55:1353–
773 1376
774 Boyer T, Antonov J, Garcia H, Johnson D, Locarnini R, Mishonov A, et al. (2006) World ocean
775 database 2005. In: Levitus S (ed) NOAA Atlas NESDIS 60, US Government Printing Office,
776 Washington, DC
777 Boyer T, Garcia H, Locarnini R, Zweng M, Mishonov A, Reagan JR, et al. (2018) World Ocean
778 Atlas 2018. Nitrate. NOAA National Centers for Environmental Information. Dataset.
779 http://www.ncei.noaa.gov/archive/accession/NCEI-WOA18. Last access: December
780 2022
781 Bracher A, Bouman HA, Brewin RJ, Bricaud A, Brotas V, Ciotti AM, et al. (2017) Obtaining
782 phytoplankton diversity from ocean color: a scientific roadmap for future development.
783 Frontiers in Marine Science 4:55. https://doi.org/10.3389/fmars.2017.00055

784 Chassot E, Bonhommeau S, Dulvy NK, Mélin F, Watson R, Gascuel D, et al. (2010) Global
785 marine primary production constrains fisheries catches. Ecology Letters 13:495–505
786 Chen Y, Tang DL (2012) Eddy-feature phytoplankton bloom induced by a tropical cyclone in
787 the South China Sea. International Journal of Remote Sensing 33:7444–7457
788 Chisholm S (1992) Phytoplankton size. In: Falkowski P, Woodhead A (eds) Primary productivity
789 and biogeochemical cycles in the sea. Plenum Press, p 213–237
790 Clayton S, Dutkiewicz S, Jahn O, Follows MJ (2013) Dispersal, eddies, and the diversity of
791 marine phytoplankton. Limnology and Oceanography: Fluids and Environments 3:182–
792 197
793 Clayton S, Dutkiewicz S, Jahn O, Hill C, Heimbach P, Follows MJ (2017) Biogeochemical versus
794 ecological consequences of modeled ocean physics. Biogeosciences 14:2877–2889
795 Cornec M, Claustre H, Mignot A, Guidi L, Lacour L, Poteau A, D'Ortenzio F, Gentili B,
796 Schmechtig C (2021) Deep chlorophyll maxima in the global ocean: occurrences, drivers
797 and characteristics. Global Biogeochemical Cycles 35:e2020GB006759.
798 https://doi.org/10.1029/2020 GB006759
799 Daly AJ, Baetens JM, De Baets B (2018) Ecological diversity: measuring the unmeasurable.
800 Mathematics 6:119. https://doi.org/10.3390/math6070119
801 Deo A, Ganer D, Nair G (2011) Tropical cyclone activity in global warming scenario. Natural
802 Hazards 59:771–786
803 Donlon CJ, Martin M, Stark J, Roberts-Jones J, Fiedler E, Wimmer W (2012) The Operational
804 Sea Surface Temperature and Sea Ice Analysis (OSTIA) system. Remote Sensing of
805 Environment 116:140–158

806 DuRand MD, Olson RJ, Chisholm SW (2001) Phytoplankton population dynamics at the
807 Bermuda Atlantic Time-series station in the Sargasso Sea. Deep Sea Research Part II:
808 Topical Studies in Oceanography 48:1983–2003
809 Dutkiewicz S, Hickman A, Jahn O, Gregg W, Mouw C, Follows M (2015) Capturing optically
810 important constituents and properties in a marine biogeochemical and ecosystem
811 model. Biogeosciences 12:4447–4481
812 Dutkiewicz S, Cermeno P, Jahn O, Follows MJ, Hickman AE, Taniguchi DA, et al. (2020)
813 Dimensions of marine phytoplankton diversity. Biogeosciences 17:609–634
814 Estrada M, Delgado M, Blasco D, Latasa M, Cabello AM, Benítez-Barrios V, et al. (2016)
815 Phytoplankton across tropical and subtropical regions of the Atlantic, Indian and Pacific
816 oceans. PloS ONE 11:e0151699. https://doi.org/10.1371/journal.pone.0151699
817 Fiedler PC, Redfern JV, Van Noord J, Hall C, Pitman RL, Ballance LT (2013) Effects of a tropical
818 cyclone on a pelagic ecosystem from the physical environment to top predators. Marine
819 Ecology Progress Series 484:1–16
820 Field CB, Behrenfeld MJ, Randerson JT, Falkowski P (1998) Primary production of the
821 biosphere: integrating terrestrial and oceanic components. Science 281:237–240
822 Follows MJ, Dutkiewicz S (2011) Modeling diverse communities of marine microbes. Annual
823 Review of Marine Science 3:427–451
824 Foltz GR, Balaguru K, Leung LR (2015) A reassessment of the integrated impact of tropical
825 cyclones on surface chlorophyll in the western subtropical North Atlantic. Geophysical
826 Research Letters 42:1158–1164
827 Garcia-Soto C, Cheng L, Caesar L, Schmidtko S, Jewett EB, Cheripka A, et al. (2021) An overview
828 of ocean climate change indicators: sea surface temperature, ocean heat content,
829 ocean pH, dissolved oxygen concentration, Arctic sea ice extent, thickness and volume,

sea level and strength of the AMOC (Atlantic Meridional Overturning Circulation). Frontiers in Marine Science. https://doi.org/10.3389/fmars.2021.642372

Garnesson P, Mangin A, Bretagnon M (2019a) Ocean colour production centre. Satellite Observation. GlobColour-Copernicus Products. Quality information document. Copernicus Marine Environment Monitoring Service. http://marine.copernicus.eu/documents/QUID/CMEMS-OC627QUID-009-030-032-033-037-081-082-083-085-086-098.pdf

Garnesson P, Mangin A, d'Andon OF, Demaria J, Bretagnon M (2019b) The CMEMS GlobColour chlorophyll a product based on satellite observation: multi-sensor merging and flagging strategies. Ocean Science 15:819–830

Geider R, La Roche J (2002) Redfield revisited: variability of C:N:P in marine microalga and its biochemical basis. European Journal of Phycology 37:1–17

Geider RJ, MacIntyre HL, Kana TM (1998) A dynamic regulatory model of photoacclimation to light, nutrient and temperature. Limnology and Oceanography 43:679–694

Gerald B (2018) A brief review of independent, dependent and one sample t-test. International Journal of Applied Mathematics and Theoretical Physics 4:50–54

Gierach MM, Subrahmanyam B (2008) Biophysical responses of the upper ocean to major Gulf of Mexico hurricanes in 2005. Journal of Geophysical Research: Oceans 113:C04029 https://doi.org/10.1029/2007JC004419

Goericke R, Welschmeyer NA (1998) Response of Sargasso Sea phytoplankton biomass, growth rates and primary production to seasonally varying physical forcing. Journal of Plankton Research 20:2223–2249

Gohin F (2011) Annual cycles of chlorophyll-a, non-algal suspended particulate matter, and turbidity observed from space and in-situ in coastal waters. Ocean Science 7:705–732

Gohin F, Druon J, Lampert L (2002) A five channel chlorophyll concentration algorithm applied to SeaWiFS data processed by SeaDAS in coastal waters. International Journal of Remote Sensing 23:1639–1661

Gordon H, McCluney W (1975) Estimation of the depth of sunlight penetration in the sea for remote sensing. Applied Optics 14:413–416

Gruber N, Keeling CD, Bates NR (2002) Interannual variability in the North Atlantic Ocean carbon sink. Science 298:2374–2378

Hickman A, Dutkiewicz S, Williams R, Follows M (2010) Modelling the effects of chromatic adaptation on phytoplankton community structure in the oligotrophic ocean. Marine Ecology Progress Series 406:1–17

Holling CS (1959) The components of predation as revealed by a study of small mammal predation on the European pine sawfly. The Canadian Entomologist 91:293–320

Hu C, Lee Z, Franz B (2012) Chlorophyll-a algorithms for oligotrophic oceans: a novel approach based on three-band reflectance difference. Journal of Geophysical Research: Oceans 117:C01011. https://doi.org/10.1029/2011JC007395

IOCCG (2014). Phytoplankton functional types from space. In: Sathyendranath S (ed) Reports of the International Ocean-Colour Coordinating Group, No. 15, Dartmouth, Canada

Irigoien X, Huisman J, Harris RP (2004) Global biodiversity patterns of marine phytoplankton and zooplankton. Nature 429:863–867

Jahn O, Hill C, Dutkiewicz S, Follows M (2019) MITgcm 3-daily global sea surface temperature, ocean currents, nitrate and phytoplankton biomass (1992–2016). UC San Diego Library Digital Collections. https://doi.org/10.6075/J0BR8QJ1

876 Jeffrey S, Vesk M (1997) Introduction to marine phytoplankton and their pigment signatures.
877 In: Jeffrey S, Mantoura R, Wright S (eds) Phytoplankton pigment in oceanography:
878 guidelines to modern methods. UNESCO Publishing, p 37–84
879 Kang D, Curchitser EN (2013) Gulf stream eddy characteristics in a high-resolution ocean
880 model. Journal of Geophysical Research: Oceans 118:4474–4487
881 Kang JJ, Min JO, Kim Y, Lee CH, Yoo HK, Jang H, Kim, MJ, et al. (2021) Vertical distribution of
882 phytoplankton community and pigment production in the Yellow Sea and the East China
883 Sea during the late summer season. Water 13:3321.
884 https://doi.org/10.3390/w13233321
885 Kimball SK, Mulekar MS (2004) A 15-year climatology of North Atlantic tropical cyclones. Part
886 I: size parameters. Journal of Climate 17:3555–3575
887 Kirk JT (2011) Light and photosynthesis in aquatic ecosystems. Cambridge University Press,
888 England
889 Kossin JP, Knapp KR, Olander TL, Velden CS (2020) Global increase in major tropical cyclone
890 exceedance probability over the past four decades. Proceedings of the National
891 Academy of Sciences 117:11975–11980
892 Kuhn A, Dutkiewicz S, Jahn O, Clayton S, Rynearson T, Mazloff M, et al. (2019) Temporal and
893 spatial scales of correlation in marine phytoplankton communities. Journal of
894 Geophysical Research: Oceans 124:9417–9438
895 Latasa M, Cabello AM, Morán X, Massana R, Scharek R (2017) Distribution of phytoplankton
896 groups within the deep chlorophyll maximum. Limnology and Oceanography 62:665–
897 685

898 Latasa M, Gutiérrez-Rodríguez A, Cabello AMM, Scharek R (2016) Influence of light and
899 nutrients on the vertical distribution of marine phytoplankton groups in the deep
900 chlorophyll maximum. Scientia Marina 80:57–62
901 Lawrence M, Avila L, Beven J, Franklin J, Pasch R, Stewart S (2005) Annual summary: Atlantic
902 hurricane season of 2003. Monthly Weather Review 133:1744–1773
903 Litchman E, Klausmeier C, Schofield O, Falkowski P (2007) The role of functional traits and
904 trade-offs in structuring phytoplankton communities: scaling from cellular to ecosystem
905 level. Ecology Letters 10:1170–1181
906 Litchman E, Tezanos Pinto P, Edwards KF, Klausmeier CA, Kremer CT, Thomas MK (2015)
907 Global biogeochemical impacts of phytoplankton: a trait-based perspective. Journal of
908 Ecology 103:1384–1396
909 Longhurst A (1995) Seasonal cycles of pelagic production and consumption. Progress in
910 Oceanography 36:77–167
911 Longhurst A (2007) Ecological geography of the sea. Academic Press. Second edition, Elsevier
912 Inc
913 Lü H, Zhao X, Sun J, Zha G, Xi J, Cai S (2020) A case study of a phytoplankton bloom triggered
914 by a tropical cyclone and cyclonic eddies. PloS ONE 15:e0230394.
915 https://doi.org/10.1371/journal.pone.0230394
916 Malone TC, Pike SE, Conley DJ (1993) Transient variations in phytoplankton productivity at
917 the JGOFS Bermuda time series station. Deep Sea Research Part I: Oceanographic
918 Research Papers 40:903–924
919 Mangesh G, Siby K, Damodar SM, Hema N, Naqvi S (2016) Cyclone Phyan-induced plankton
920 community succession in the coastal waters off Goa, India. Current Science 11:1091–
921 1097

922 Mao Y, Sun J, Guo C, Wei Y, Wang X, Yang S, et al. (2019) Effects of Typhoon Roke and Haitang
923 on phytoplankton community structure in northeastern South China Sea. Ecosystem
924 Health and Sustainability 5:144–154
925 Marañon E, Cermeño P, López-Sandoval D, Rodríguez-Ramos T, Sobrino C, Huete-Ortega M,
926 et al. (2013) Unimodal size scaling of phytoplankton growth and the size dependence of
927 nutrient uptake and use. Ecology Letters 16:371–379
928 Marshak AR, Link JS (2021) Primary production ultimately limits fisheries economic
929 performance. Scientific Reports 11:1–10
930 Marshall J, Adcroft A, Hill C, Perelman L, Heisey C (1997) A finite-volume, incompressible
931 Navier Stokes model for studies of the ocean on parallel computers. Journal of
932 Geophysical Research: Oceans 102:5753–5766
933 Mei W, Pasquero C (2013) Spatial and temporal characterization of sea surface temperature
934 response to tropical cyclones. Journal of Climate 26:3745–3765
935 Mei W, Pasquero C, Primeau F (2012) The effect of translation speed upon the intensity of
936 tropical cyclones over the tropical ocean. Geophysical Research Letters 39:L07801.
937 https://doi.org/10.1029/2011GL050765
938 Menemenlis D, Hill C, Adcroft A, Campin J, Cheng B, Ciotti B, et al. (2005) NASA supercomputer
939 improves prospects for ocean climate research. Eos 86:89–96
940 Menemenlis D, Campin J-M, Heimbach P, Hill C, Lee T, Nguyen A, et al. (2008) ECCO2: high
941 resolution global ocean and sea ice data synthesis. Mercator Ocean Quarterly
942 Newsletter 31:13–21
943 Menkes CE, Lengaigne M, Lévy M, Éthé C, Bopp L, Aumont O, et al. (2016) Global impact of
944 tropical cyclones on primary production. Global Biogeochemical Cycles 30:767–786

945 Mikaelyan AS, Pautova LA, Chasovnikov VK, Mosharov SA, Silkin VA (2015) Alternation of
946 diatoms and coccolithophores in the north-eastern Black Sea: a response to nutrient
947 changes. Hydrobiologia 755:89–105
948 Moeller HV, Laufkötter C, Sweeney EM, Johnson MD (2019) Light-dependent grazing can drive
949 formation and deepening of deep chlorophyll maxima. Nature Communications
950 10:1978. https://doi.org/10.1038/s41467-019-09591-2
951 Moore C, Mills M, Arrigo K, Berman-Frank I, Bopp L, Boyd P, et al. (2013) Processes and
952 patterns of oceanic nutrient limitation. Nature Geoscience 6:701–710
953 Moore CM, Mills MM, Langlois R, Milne A, Achterberg EP, La Roche J, et al. (2008) Relative
954 influence of nitrogen and phosphorous availability on phytoplankton physiology and
955 productivity in the oligotrophic sub-tropical North Atlantic Ocean. Limnology and
956 Oceanography 53:291–305
957 Morison F, Harvey E, Franzè G, Menden-Deuer S (2019) Storm-induced predator-prey
958 decoupling promotes springtime accumulation of North Atlantic phytoplankton.
959 Frontiers in Marine Science 6:608. https://doi.org/10.3389/fmars.2019.00608
960 Morozov EG, Velarde MG (2008) Inertial oscillations as deep ocean response to hurricanes.
961 Journal of Oceanography 64:495–509
962 Naik H, Naqvi S, Suresh T, Narvekar P (2008) Impact of a tropical cyclone on biogeochemistry
963 of the central Arabian Sea. Global Biogeochemical Cycles 22:GB3020.
964 https://doi.org/10.1029/2007GB003028
965 Otero J, Álvarez-Salgado XA, Bode A (2020) Phytoplankton diversity effect on ecosystem
966 functioning in a coastal upwelling system. Frontiers in Marine Science 7:592255.
967 https://doi.org/10.3389/fmars.2020.592255

968 Painter SC, Finlay M, Hemsley VS, Martin AP (2016) Seasonality, phytoplankton succession
969 and the biogeochemical impacts of an autumn storm in the northeast Atlantic Ocean.
970 Progress in Oceanography 142:72–104
971 Partensky F, Blanchot J, Vaulot D (1999a) Differential distribution and ecology of
972 *Prochlorococcus* and *Synechococcus* in oceanic waters: a review. Bulletin-Institut
973 Oceanographique Monaco – Numero Special 19:457–476
974 Partensky F, Hess WR, Vaulot D (1999b) *Prochlorococcus*, a marine photosynthetic prokaryote
975 of global significance. Microbiology and Molecular Biology Reviews 63:106–127.
976 Pasch R, Blake E, Brown D (2003) Tropical Cyclone Report Hurricane Fabian, 27 August–8
977 September 2003. National Hurricane Center, https://www.nhc.noaa.gov/data/tcr
978 Pedrosa-Pàmies R, Conte M, Weber J, Johnson R (2019) Hurricanes enhance labile carbon
979 export to the deep ocean. Geophysical Research Letters 46:10484–10494
980 Pinckney J, Richardson T (2016) Phytoplankton biodiversity in the oligotrophic northwestern
981 Sargasso Sea. In: Glibert P, Kana T (eds) Aquatic microbial ecology and biogeochemistry:
982 a dual perspective. Springer, Cham, p 239–250
983 Platt T, Bouman H, Devred E, Fuentes-Yaco C, Sathyendranath S (2005) Physical forcing and
984 phytoplankton distributions. Scientia Marina 69:55–73
985 Poulton AJ, Holligan PM, Charalampopoulou A, Adey TR (2017) Coccolithophore ecology in
986 the tropical and subtropical Atlantic Ocean: new perspectives from the Atlantic
987 meridional transect (AMT) programme. Progress in Oceanography 158:150–170
988 Price JF (1981) Upper ocean response to a hurricane. Journal of Physical Oceanography
989 11:153–175

990 Price JF, Morzel J, Niiler PP (2008) Warming of SST in the cool wake of a moving hurricane.
991 Journal of Geophysical Research: Oceans 113:C07010.
992 https://doi.org/10.1029/2007JC004393
993 Redfield AC (1958) The biological control of chemical factors in the environment. American
994 Scientist 46:205–221
995 Richardson P (1985) Drifting derelicts in the North Atlantic 1883–1902. Progress in
996 Oceanography 14:463–483
997 Rohr T, Richardson AJ, Lenton A, Shadwick E (2022) Recommendations for the formulation of
998 grazing in marine biogeochemical and ecosystem models. Progress in Oceanography
999 208:102878 https://doi.org/10.1016/j.pocean.2022.102878
1000 Shimoda Y, Arhonditsis GB (2016) Phytoplankton functional type modelling: running before
1001 we can walk? A critical evaluation of the current state of knowledge. Ecological
1002 Modelling 320:29–43
1003 Shropshire T, Li Y, He R (2016) Storm impact on sea surface temperature and chlorophyll *a* in
1004 the Gulf of Mexico and Sargasso Sea based on daily cloud-free satellite data
1005 reconstructions. Geophysical Research Letters 43:12199–12207
1006 Smith TA, Jolliff JK, Walker ND, Anderson S (2019) Biophysical submesoscale processes in the
1007 wake of Hurricane Ivan: simulations and satellite observations. Journal of Marine
1008 Science and Engineering 7:378. https://doi.org/10.3390/jmse7110378
1009 Son S, Platt T, Fuentes-Yaco C, Bouman H, Devred E, Wu Y, et al. (2007) Possible
1010 biogeochemical response to the passage of Hurricane Fabian observed by satellites.
1011 Journal of Plankton Research 29:687–697
1012 Stanichny SV, Kubryakova EA, Kubryakov AA (2021) Quasi-tropical cyclone caused anomalous
1013 autumn coccolithophore bloom in the Black Sea. Biogeosciences 18:3173–3188

1014 Steinberg DK, Carlson CA, Bates NR, Johnson RJ, Michaels AF, Knap AH (2001) Overview of the
1015 US JGOFS Bermuda Atlantic Time-series Study (BATS): a decade-scale look at ocean
1016 biology and biogeochemistry. Deep Sea Research Part II 48:1405–1477
1017 Striebel M, Singer G, Stibor H, Andersen T (2012) "Trophic overyielding": phytoplankton
1018 diversity promotes zooplankton productivity. Ecology 93:2719–2727
1019 Thierstein H, Young J (2004) Coccolithophores – from molecular processes to global impact.
1020 Springer-Verlag, Berlin
1021 Vallina SM, Follows M, Dutkiewicz S, Montoya JM, Cermeno P, Loreau M (2014) Global
1022 relationship between phytoplankton diversity and productivity in the ocean. Nature
1023 Communications 5:4299. https://doi.org/10.1038/ncomms5299
1024 Visintini N, Martiny AC, Flombaum P (2021) *Prochlorococcus*, *Synechococcus*, and
1025 picoeukaryotic phytoplankton abundances in the global ocean. Limnology and
1026 Oceanography Letters 6:207–215
1027 Walker ND, Leben RR, Balasubramanian S (2005) Hurricane-forced upwelling and chlorophyll
1028 a enhancement within cold-core cyclones in the Gulf of Mexico. Geophysical Research
1029 Letters 32:L18610. https://doi.org/10.1029/2005GL023716
1030 Ward B, Dutkiewicz S, Jahn O, Follows M (2012) A size-structured food-web model for the
1031 global ocean. Limnology and Oceanography 57:1877–1891
1032 Whitt DB, Lévy M, Taylor JR (2019) Submesoscales enhance storm-driven vertical mixing of
1033 nutrients: insights from a biogeochemical large eddy simulation. Journal of Geophysical
1034 Research: Oceans 124:8140–8165
1035 Zedler S, Dickey T, Doney S, Price J, Yu X, Mellor G (2002) Analyses and simulations of the
1036 upper ocean's response to Hurricane Felix at the Bermuda Testbed Mooring site: 13–23

August 1995. Journal of Geophysical Research: Oceans 107:3232. https://doi.org/10.1029/2001JC000969

Zhang H, He H, Zhang W-Z, Tian D (2021) Upper ocean response to tropical cyclones: a review. Geoscience Letters 8:1. https://doi.org/10.1186/s40562-020-00170-8

Zhao H, Tang D, Wang Y (2008) Comparison of phytoplankton blooms triggered by two typhoons with different intensities and translation speeds in the South China Sea. Marine Ecology Progress Series 365:57–65

Zwirglmaier K, Jardillier L, Ostrowski M, Mazard S, Garczarek L, Vaulot D, et al. (2008) Global phylogeography of marine *Synechococcus* and *Prochlorococcus* reveals a distinct partitioning of lineages among oceanic biomes. Environmental Microbiology 10:147–161

FIGURES

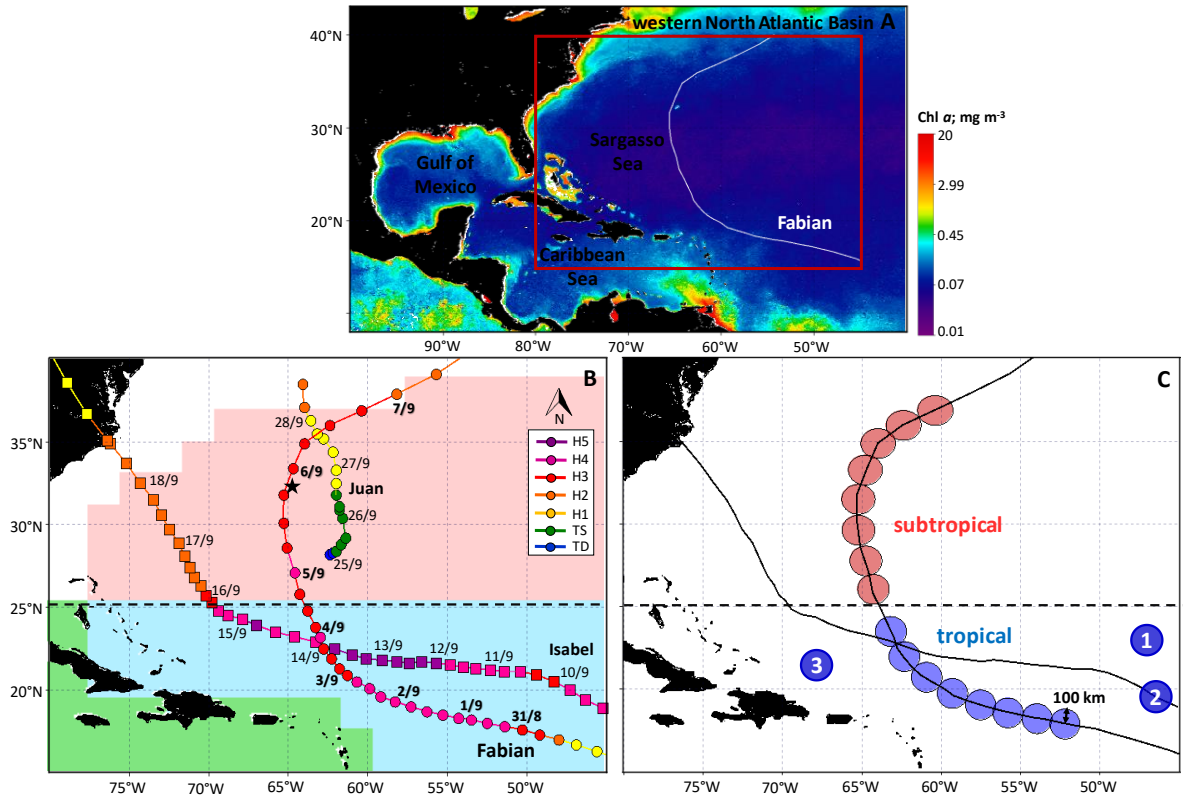

Figure 1. (A) Composite satellite chlorophyll (Chl) *a* concentration (September 1998–2002) in the western North Atlantic Basin with the study area in the Sargasso Sea delineated by the red rectangle and the trajectory of Hurricane Fabian (2003) superimposed. (B) Trajectory of Hurricanes Fabian, Isabel and Juan (2003). Colours indicate the tropical cyclone category (i.e. TD: tropical depression, TS: tropical storm and H1–H5: Saffir-Simpson Hurricane Scale based on the hurricane's maximum sustained wind speed. H1: 119–153 km h^{-1}, H2: 154–177 km h^{-1}, H3: 178–208 km h^{-1}, H4: 209–251 km h^{-1} and H5: 252 km h^{-1} or higher according to the National Hurricane Center (https://www.nhc.noaa.gov/aboutsshws.php, last access: October 2021)). Numbers along the trajectory of Fabian (bold numbers), Isabel, and Juan indicate the day/month. The black star indicates the location of Bermuda island. The shaded pink, blue and green areas indicate the North Atlantic Subtropical Gyral (West), the North Atlantic Tropical Gyral and the Caribbean biogeochemical provinces of Longhurst (1995), respectively. (C) 100 km radius disks centered at some hurricane positions along Fabian's trajectory in the tropical and subtropical waters separately. The dark blue disks 1, 2 and 3 indicate areas not affected by hurricane forcing (disks 1 and 3) and affected by Hurricane Isabel (disk 2) where the post-storm biological and chemical responses were also investigated. The black dashed lines denote the 25° N latitude separating tropical and subtropical waters.

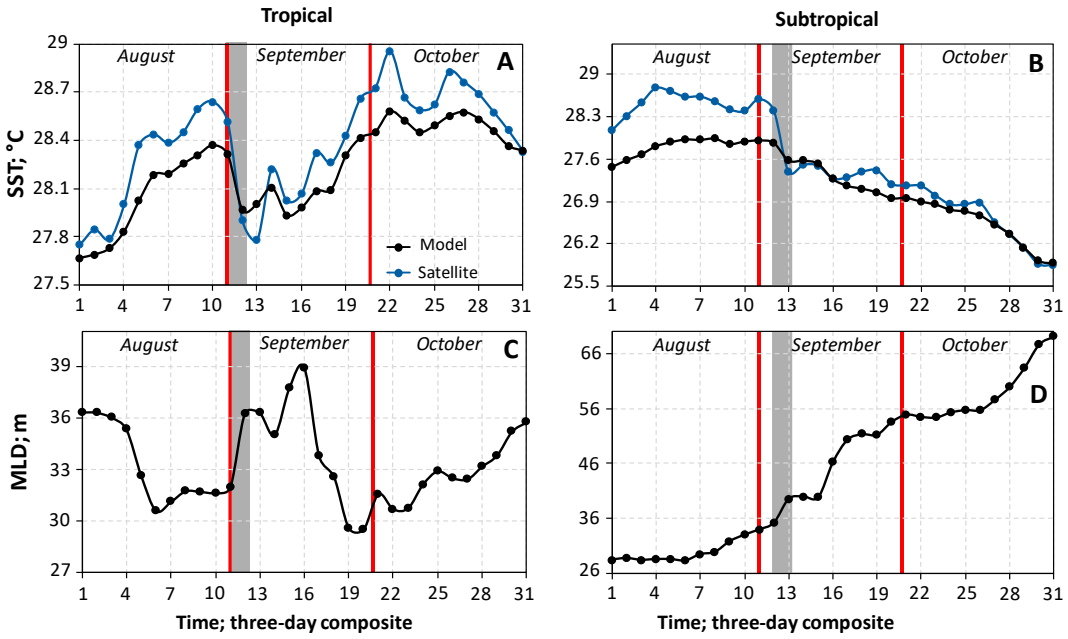

1067

1068 **Figure 2.** Temporal evolution of three-day composite modelled and satellite sea surface
1069 temperature (SST) data in the (A) tropical and (B) subtropical waters along Fabian's trajectory.
1070 Modelled mixed layer depth (MLD) in the (C) tropical and (D) subtropical waters along
1071 Fabian's trajectory. The vertical red lines enclose the months of August–October (2003), and
1072 the grey-shaded area marks the days Fabian affected the area.

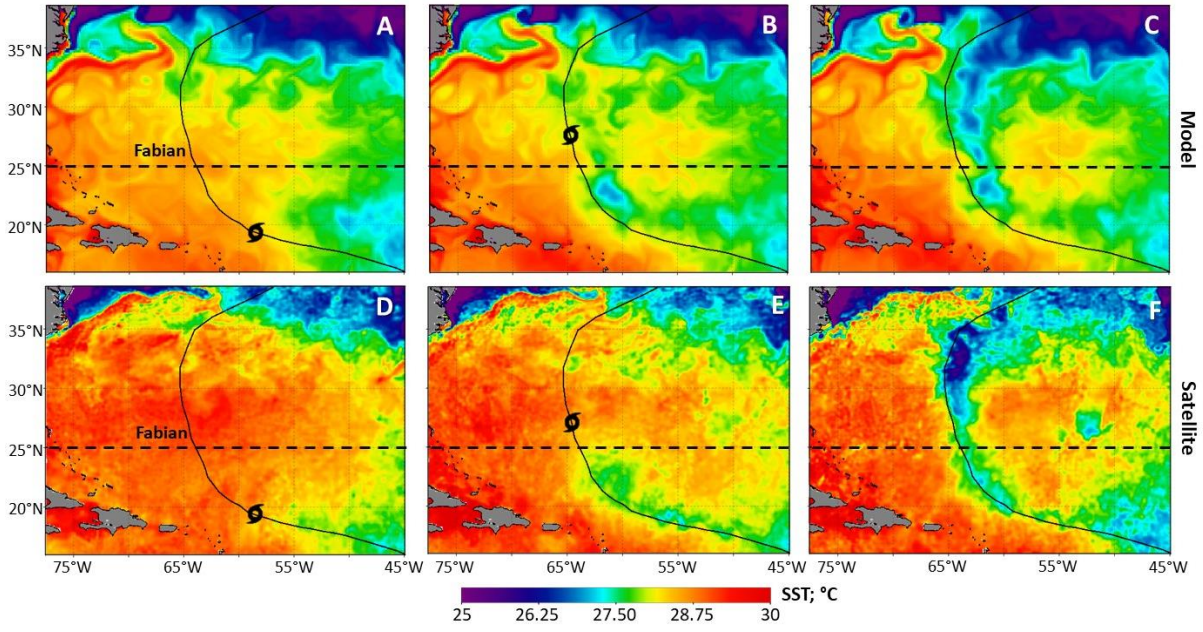

1073

Figure 3. Three-day composite (A–C) modelled and (D–F) satellite sea surface temperature (SST) data. (A and D) three-day composite 11 (August 31-September 2) when Fabian started to affect the tropical waters, (B and E) three-day composite 12 (September 3–5) when Fabian started to affect the subtropical waters, and (C and F) three-day composite 13 (September 6–8) when Fabian left the study area. The trajectory of Fabian and a hurricane symbol indicating the position of Fabian during the last day of the corresponding three-day composite are superimposed. The black dashed lines denote the 25° N latitude separating tropical and subtropical waters.

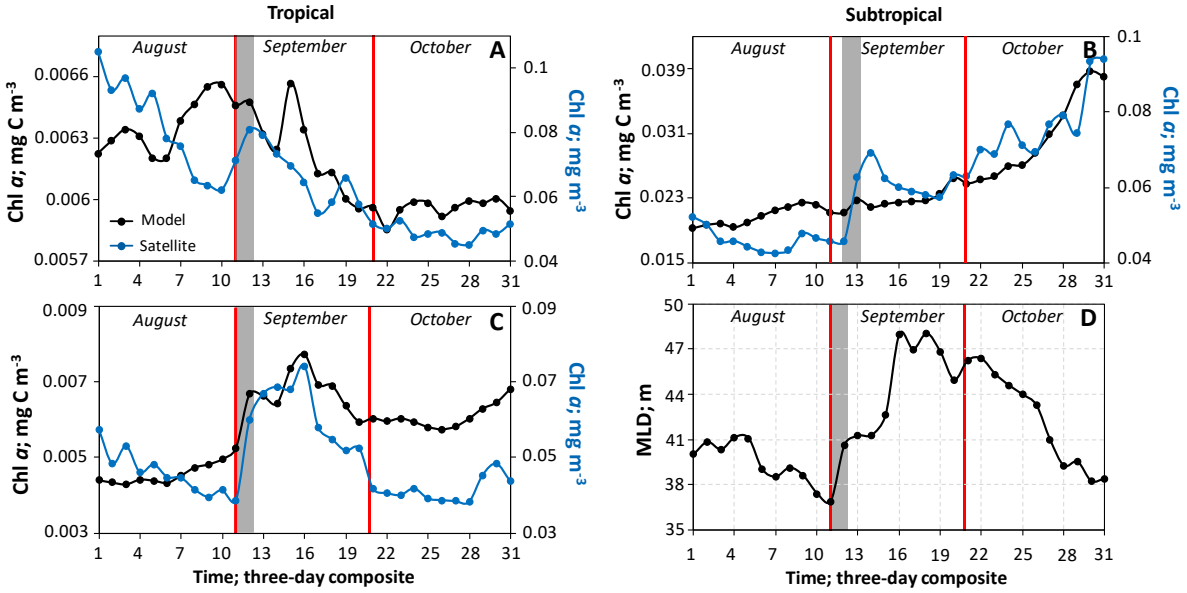

Figure 4. Temporal evolution of three-day composite modelled and satellite chlorophyll (Chl) *a* concentration data in the (A) tropical and (B) subtropical waters along Fabian's trajectory. (C and D) depict the local Chl *a* concentration and mixed layer depth (MLD) responses, respectively, in the area delineated by the disk in Fig. 5. The vertical red lines enclose the months of August–October (2003), and the grey-shaded area marks the days Fabian affected the area.

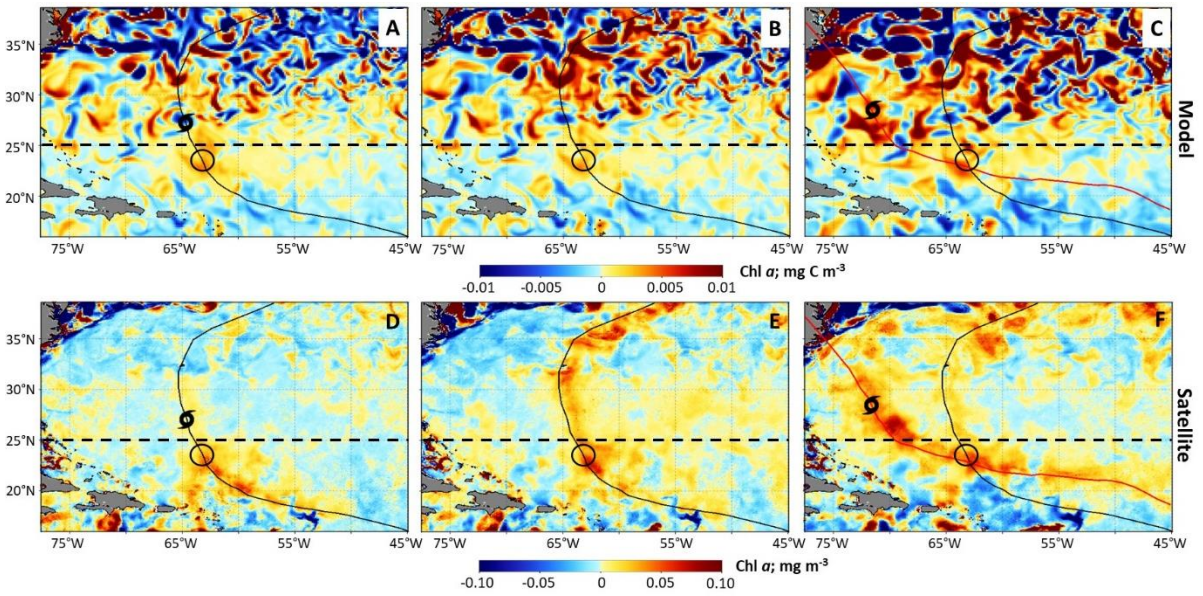

1089

1090 **Figure 5.** Three-day composite (A–C) modelled and (D–F) satellite chlorophyll (Chl) *a*
1091 concentration anomalies. Anomalies of (A and D) three-day composite 12 (September 3–5)
1092 when Fabian started to affect the tropical waters, (B and E) three-day composite 13
1093 (September 6–8) when Fabian started to affect the subtropical waters, and (C and F) three-
1094 day composite 16 (September 15–17) accounting for the passage of Isabel. The trajectory of
1095 Fabian and a hurricane symbol indicating the position of Fabian and Isabel during the last day
1096 of the corresponding three-day composite are superimposed. The black dashed lines denote
1097 the 25° N latitude separating tropical and subtropical waters.

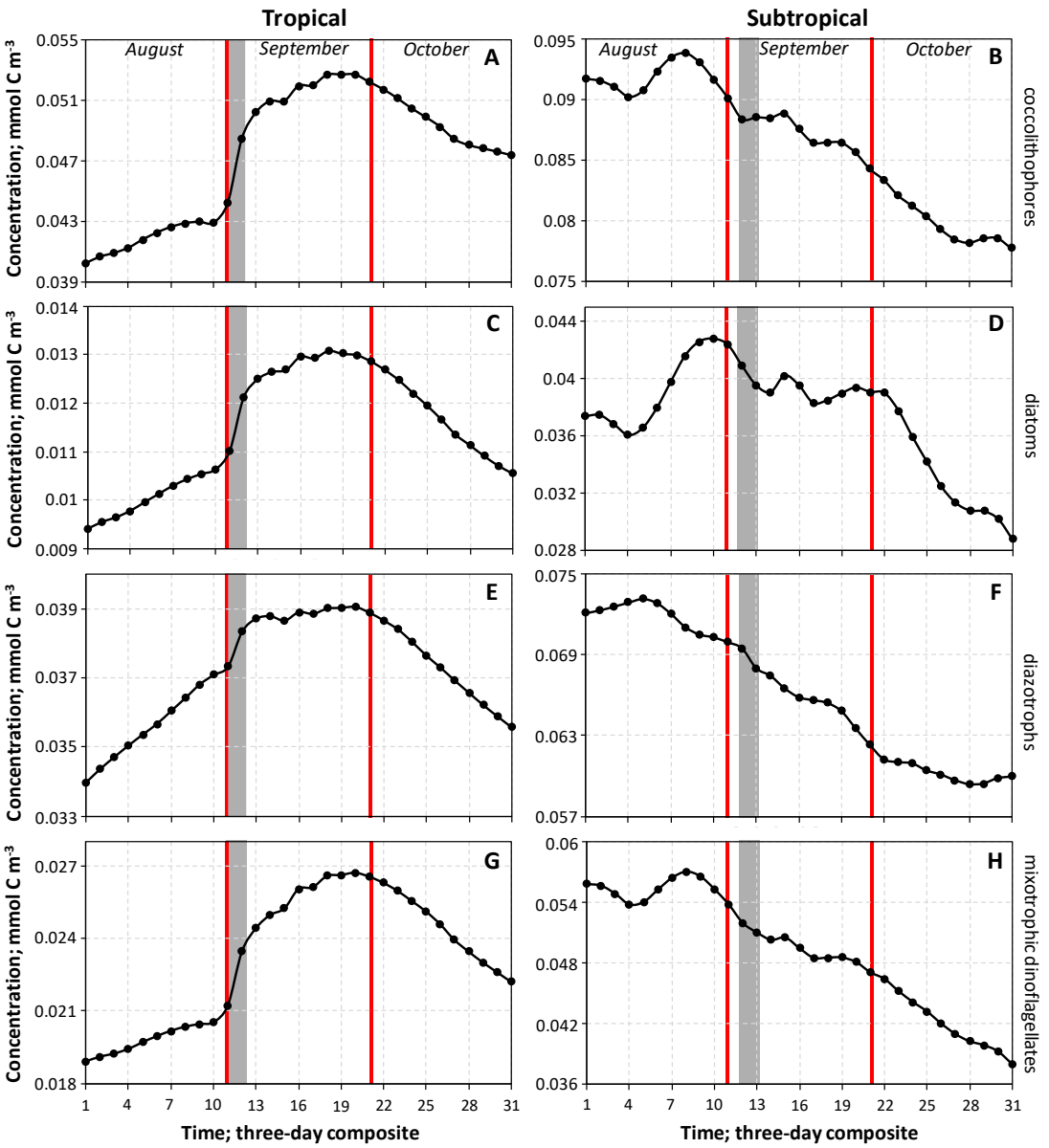

Figure 6. Temporal evolution of three-day mean concentration in the euphotic zone (0–200 m) of the phytoplankton functional types (PFTs): coccolithophores, diatoms, diazotrophs, mixotrophic dinoflagellates, picoeukaryotes, *Prochlorococcus* and *Synechococcus* in the tropical and subtropical waters along the trajectory of Fabian. Different y-axis ranges allow to better highlight the temporal variability of each PFT in each study area. The vertical red lines enclose the months of August–October (2003), and the grey-shaded area marks the days Fabian affected the area.

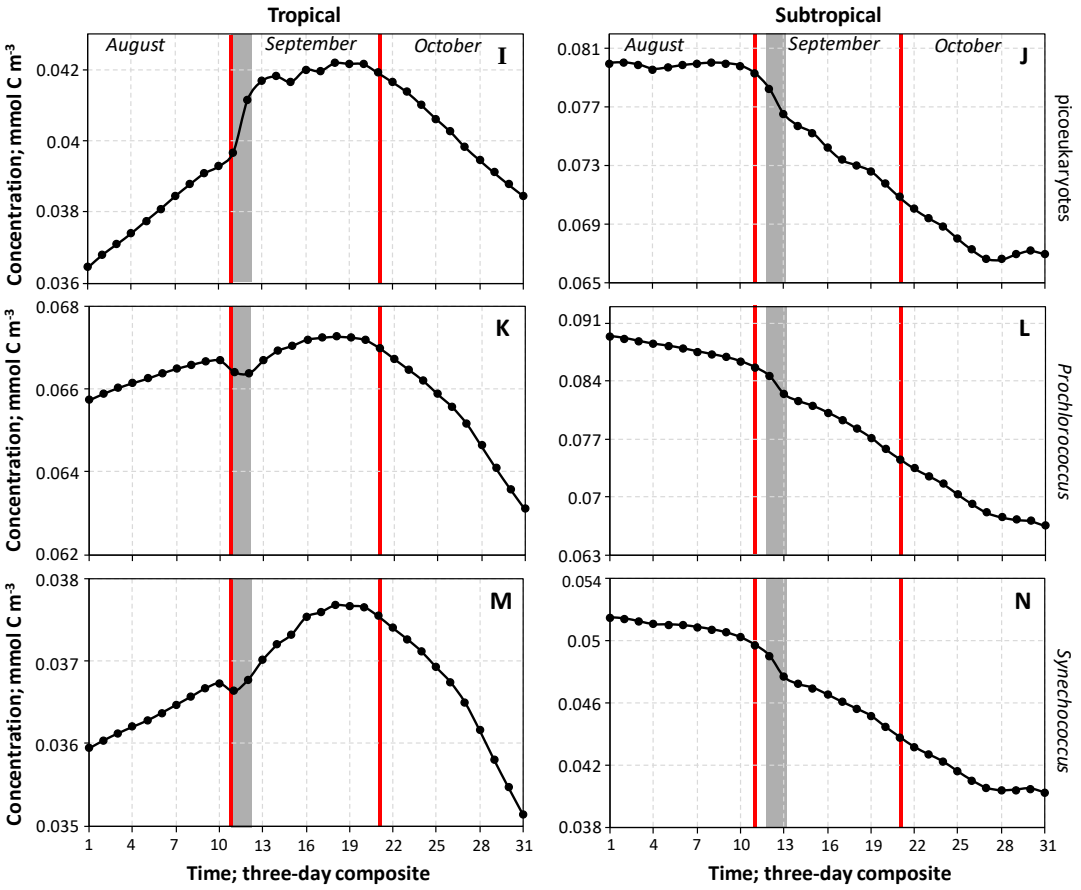

1106

1107 **Figure 6.** Continuation.

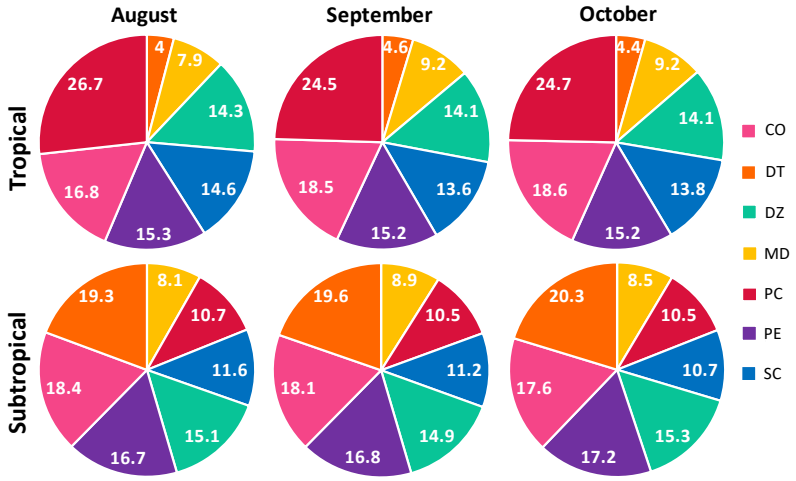

1108

1109 **Figure 7.** Proportion of each phytoplankton functional type (PFT) concentration to the total

1110 phytoplankton concentration in the tropical and subtropical waters crossed by Fabian (2003).

1111 Coccolithophores (CO), diatoms (DT), diazotrophs (DZ), mixotrophic dinoflagellates (MD),

1112 picoeukaryotes (PE), *Prochlorococcus* (PC) and *Synechococcus* (SC).

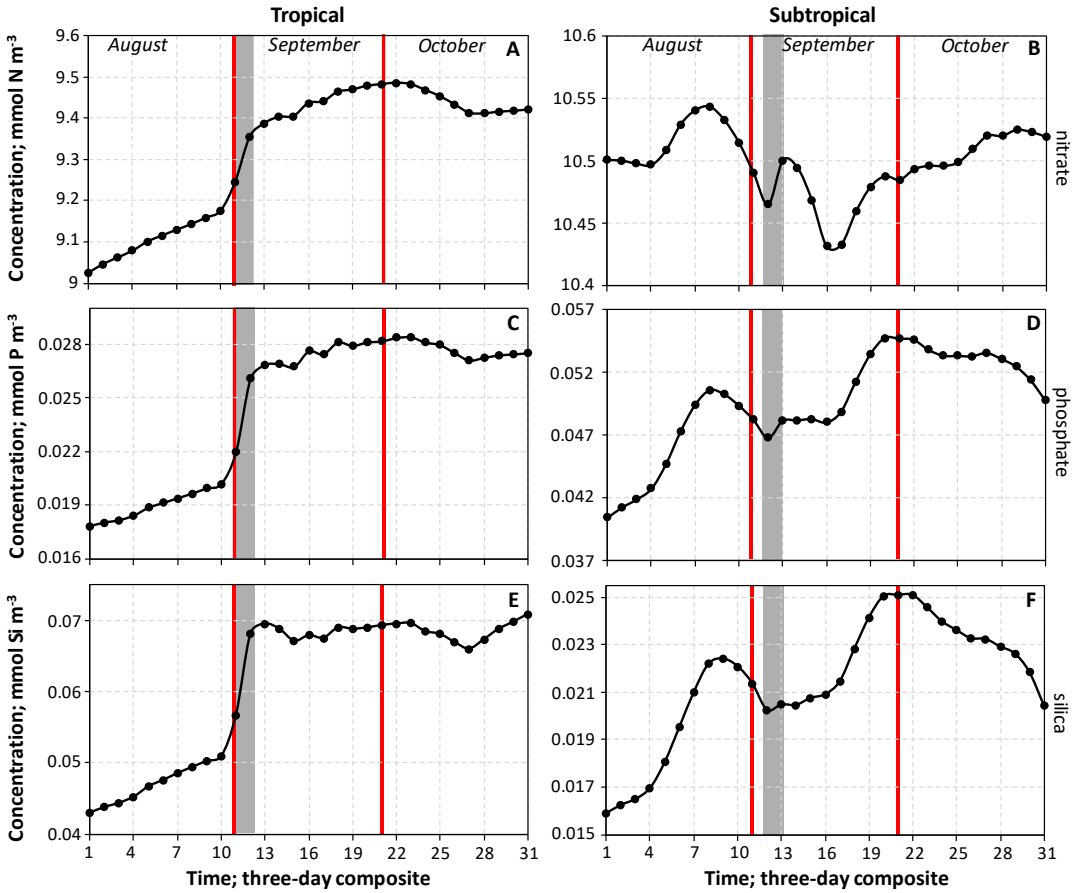

1113

1114 **Figure 8.** Like Fig. 6 but for the nitrate, phosphate and silica concentrations.

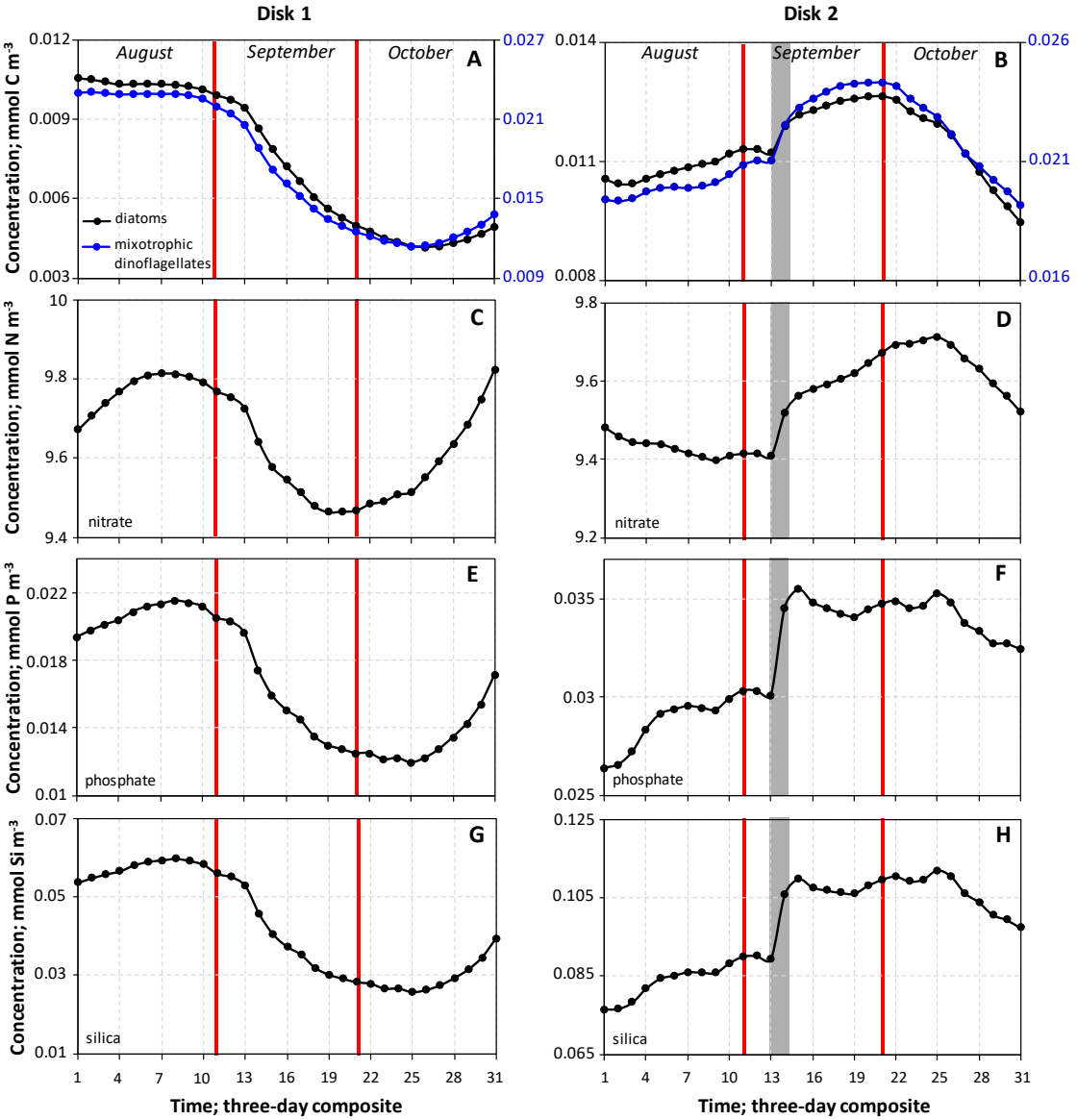

Figure 9. Temporal evolution of three-day mean concentration in the euphotic zone (0–200 m) of (A and B) diatoms and mixotrophic dinoflagellates, (C and D) nitrate, (E and F) phosphate, and (G and H) silica concentrations in the disks 1 and 2 represented in Fig. 1C. Different y-axis ranges allow to better highlight the temporal variability of each phytoplankton functional type (PFT) in each study area. The vertical red lines enclose the months of August–October (2003), and the grey-shaded area marks the days Isabel affected the area as well as the immediate oceanic response induced.

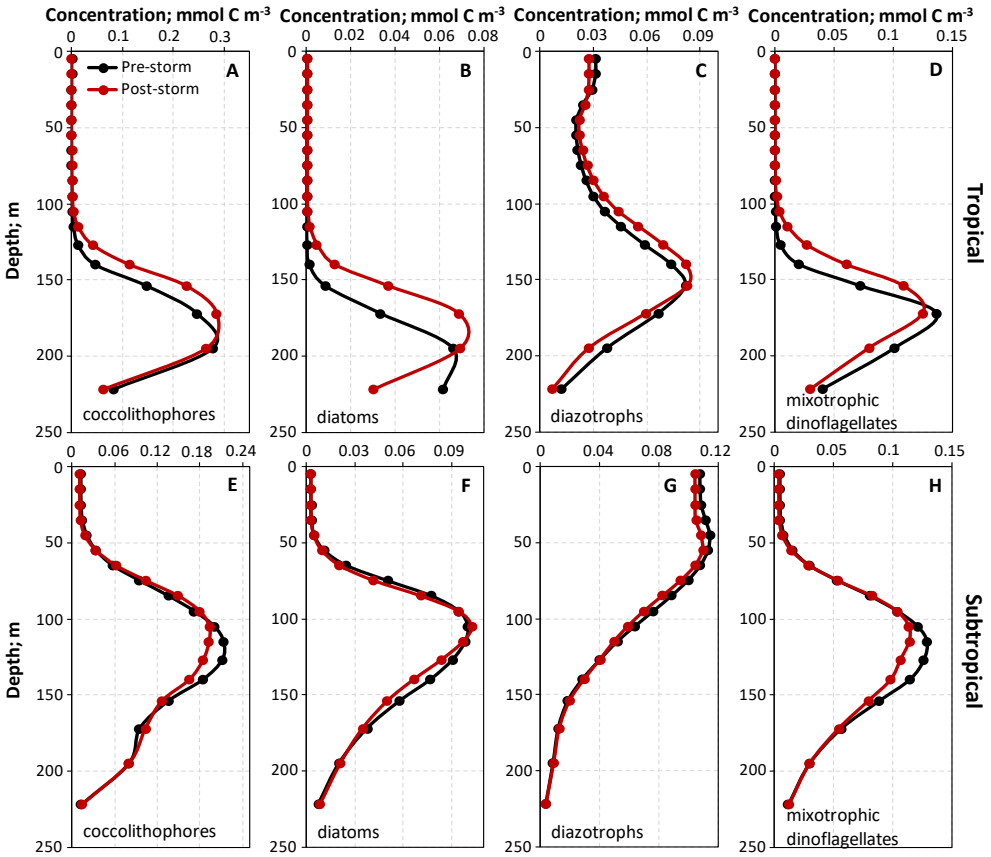

Figure 10. Profiles of phytoplankton functional type (PFT) concentrations: coccolithophores, diatoms, diazotrophs, mixotrophic dinoflagellates, picoeukaryotes, *Prochlorococcus* and *Synechococcus* in the tropical and subtropical waters along the trajectory of Fabian before and after its passage. Different x-axis ranges allow to better highlight the spatial variability of each PFT in each study area.

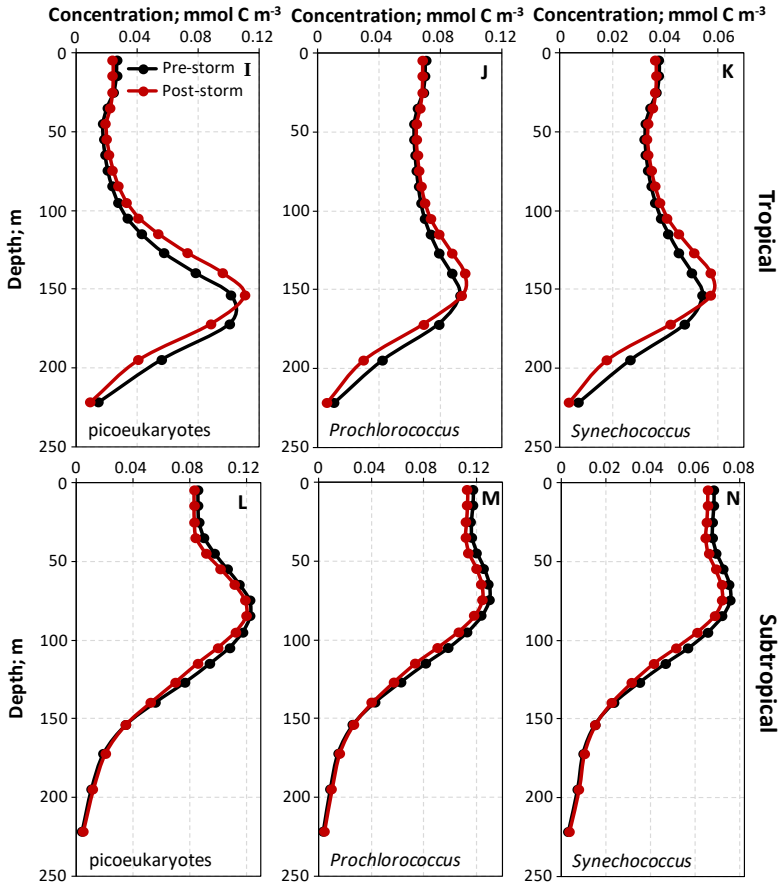

1129

1130 **Figure 10.** Continuation.

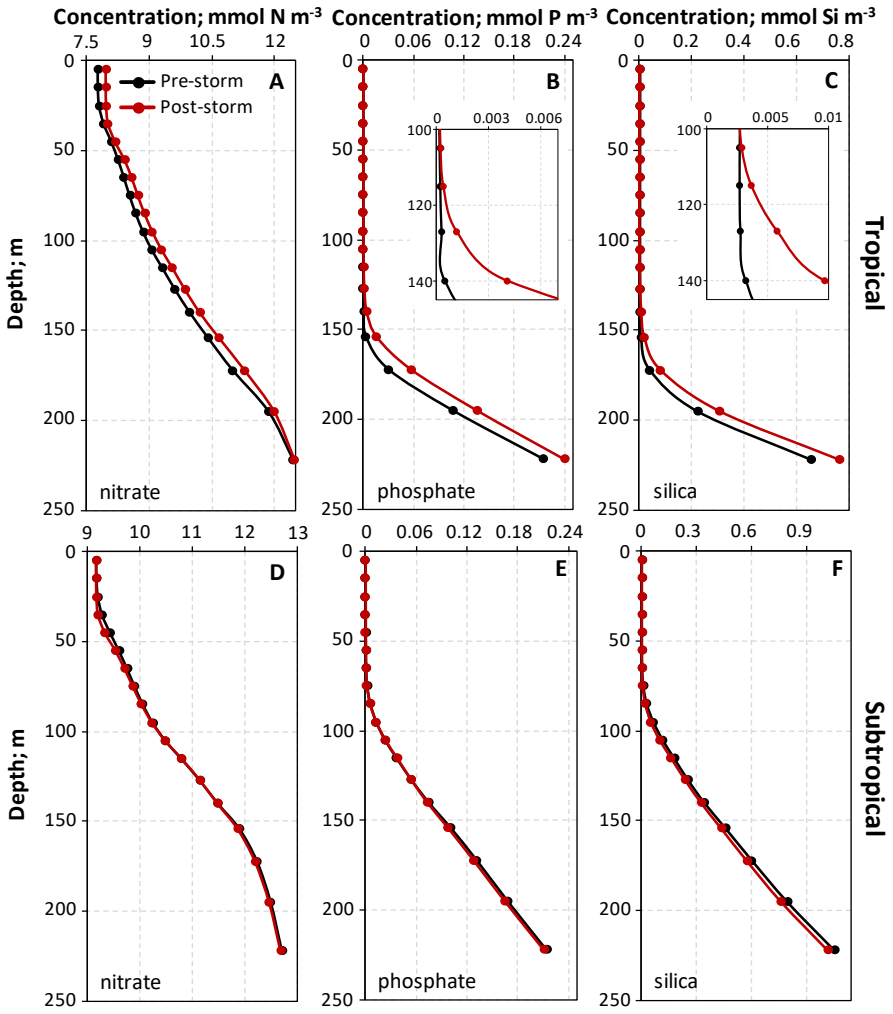

1131

1132 **Figure 11.** Like Fig. 10 but for the nitrate, phosphate and silica concentrations. The small

1133 graphics in (B) and (C) show the profiles in the upper ocean layer using a finer scale in order

1134 to highlight the differences between pre-storm and post-storm concentrations.

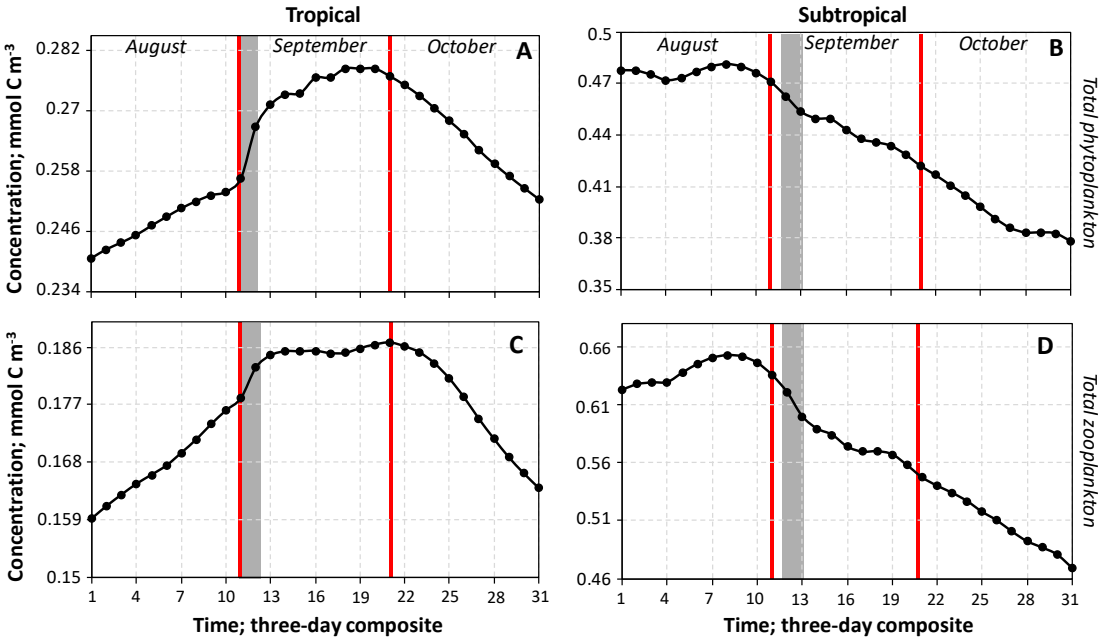

1135

1136 **Figure 12.** Like Fig. 6 but for the total phytoplankton and zooplankton concentrations.

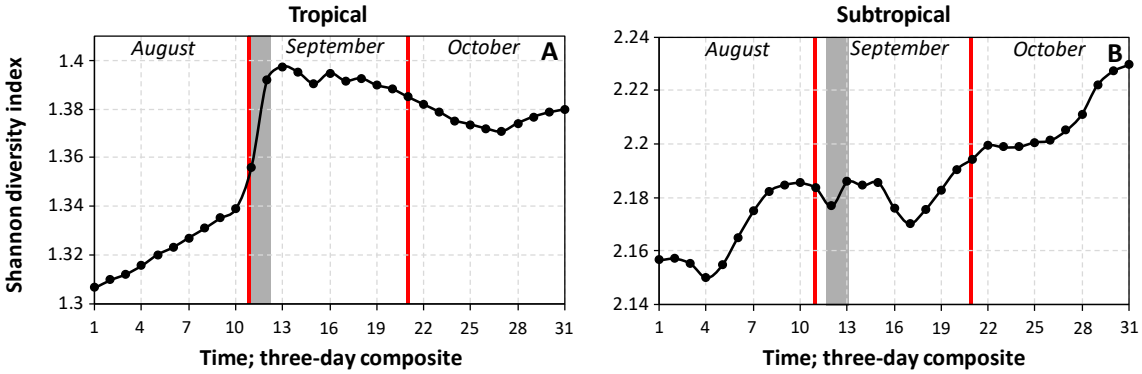

1137

1138 **Figure 13.** Like Fig. 6 but for the Shannon diversity index.